Original Article

Development and experimental validation of a senescence-related long non-coding RNA signature for prognostic prediction and immune microenvironment characterization in gastric cancer patients

Jinglong Shi[1#], Zehui Hou[2,3,4#], Ludi Fan[5], Chen Hu[1], Ning Ma[2,3,4], Enmin Huang[2,3,4]

[1]Department of General Surgery, Guangzhou Twelfth People's Hospital, Guangzhou, China; [2]Department of Gastroenterological Surgery and Hernia Center, The Sixth Affiliated Hospital, Sun Yat-sen University, Guangzhou, China; [3]Guangdong Provincial Key Laboratory of Colorectal and Pelvic Floor Diseases, The Sixth Affiliated Hospital, Sun Yat-sen University, Guangzhou, China; [4]Biomedical Innovation Center, The Sixth Affiliated Hospital, Sun Yat-sen University, Guangzhou, China; [5]Department of Guang Yuan Internal Medicine, Guangzhou Twelfth People's Hospital, Guangzhou, China

Contributions: (I) Conception and design: E Huang, N Ma; (II) Administrative support: E Huang, N Ma; (III) Provision of study materials or patients: J Shi, Z Hou; (IV) Collection and assembly of data: J Shi, Z Hou; (V) Data analysis and interpretation: J Shi, Z Hou, L Fan, C Hu; (VI) Manuscript writing: All authors; (VII) Final approval of manuscript: All authors.

[#]These authors contributed equally to this work.

Correspondence to: Enmin Huang, MD, PhD; Ning Ma, MD, PhD. Department of Gastroenterological Surgery and Hernia Center, The Sixth Affiliated Hospital, Sun Yat-sen University, Guangzhou, China; Guangdong Provincial Key Laboratory of Colorectal and Pelvic Floor Diseases, The Sixth Affiliated Hospital, Sun Yat-sen University, Guangzhou, China; Biomedical Innovation Center, The Sixth Affiliated Hospital, Sun Yat-sen University, No. 26, Yuancun Erheng Road, Tianhe District, Guangzhou 510655, China. Email: huangenm5@mail.sysu.edu.cn; maning9@mail.sysu.edu.cn.

Background: Cellular senescence is considered a new marker of cancer. It has been suggested that long non-coding RNA (lncRNA) can be used to predict the prognosis of cancers. However, it remains to be seen whether the lncRNAs associated with cellular senescence can be used to predict the prognosis of gastric cancer (GC). The present study aimed to develop a novel senescence-related lncRNA signature (SenLncSig) to predict GC prognosis. The SenLncSig model holds promise for enhancing patient stratification, enabling more precise prognostic predictions and facilitating immunotherapy strategies.

Methods: Senescence-associated lncRNAs were identified from RNA expression profiles in The Cancer Genome Atlas (TCGA) database through the construction of a co-expression network linking senescence genes and lncRNAs. A prognostic signature for GC (334 patients from TCGA-STAD data set), comprising the senescence-related lncRNAs, was developed through univariate and multivariate Cox proportional hazards regression analyses. By using the median SenLncSig risk score, the GC patients were categorized into high- and low-risk groups. A Kaplan-Meier analysis and gene set enrichment analysis were conducted, and immune infiltration, the tumor mutation burden (TMB), and pharmacological treatments were compared between the high- and low-risk groups. We used an independent GC cohort (an external cohort of 30 pairs of tumor and non-tumor tissues from the GC patients) and three GC cell lines to conduct a quantitative reverse-transcription polymerase chain reaction (qRT-PCR) analysis to validate the results.

Results: We established a SenLncSig, a prognostic risk model comprising the following five senescence-associated lncRNAs; AP000695.2, LINC02381, AC005586.1, AP003392.1, and AP001528.2. According to the SenLncSig, high-risk scores were associated with poor overall survival (multivariate Cox proportional hazard ratio: 1.498, 95% confidence interval: 1.294–1.735; P<0.001). The time-dependent receiver operating characteristic curve indicated that the model performed (area under the curve: 0.711). We developed a nomogram incorporating age, gender, grade, stage, T stage, M stage, N stage, and SenLncSig risk score to estimate 1-year, 3-year, and 5-year survival rates. Further, according to the results of the mutation analysis, patients with a high TMB in the high-risk group had the worst prognosis. Interestingly, the high-risk group

had a stronger infiltration of regulatory T cells (P<0.001) and M2 macrophage cells (P<0.001), as well as higher tumor immune dysfunction and exclusion scores than the low-risk group. These results might explain why the high-risk group had a worse prognosis. Finally, the qRT-PCR validation revealed that the AP000695.2 and AP003392.1 expression levels were significantly higher in the tumor tissues and GC cell lines than the normal tissues and normal human gastric epithelial cell line, whereas the opposite pattern was found for LINC02381.

Conclusions: The development of the SenLncSig provided a potential tool for improving patient prognosis predictions and offered preliminary insights into predicting the efficacy of GC immunotherapy.

Keywords: Gastric cancer (GC); cellular senescence; long non-coding RNA (lncRNA); prognosis; immunotherapy

Submitted Oct 19, 2024. Accepted for publication Dec 18, 2024. Published online Dec 26, 2024.
doi: 10.21037/jgo-24-792
View this article at: https://dx.doi.org/10.21037/jgo-24-792

Introduction

Gastric cancer (GC) is the second leading cause of cancer death (1). It has been estimated that 23.7% of the global total of GC cases and 30.2% of GC-related deaths occur in China (2). In China, less than 15% of early stage patients have a high survival rate, while half (54%) of patients with locally advanced disease have a low 5-year survival rate (3). Randomized clinical trials have provided evidence that combined modality therapy is essential for patients with locally advanced disease (4). To date, only three molecular biomarkers have been validated for predicting the efficacy of systemic therapies in GC patients; that is, HER2 positivity for trastuzumab, microsatellite instability status, and programmed death-ligand 1 (PD-L1) expression for pembrolizumab (5). Most patients with advanced disease respond poorly to these therapies due to the lack of appropriate biomarkers (5).

There is extensive evidence that cellular senescence prevents cancer (6,7). Further, there is increasing evidence that senescent cells, especially those that form part of the tumor microenvironment (TME), may be involved in tumor formation and development under certain conditions (8). For example, senescent stromal cells that secrete senescence-associated secretory proteins (SASPs), such as IL-6, IL-8, and IL-10, contribute to tumor progression and metastasis (9). In a senescent TME, the proliferation of immunosuppressive cells, such as myeloid suppressor cells and T regulatory cells (Tregs) is accelerated, while the activity of effector T cells, natural killer (NK) cells, macrophages, and dendritic cells (DCs) is significantly reduced, promoting tumorigenic immune escape (10). However, the function of senescent cells in the GC TME is unclear.

Long non-coding RNAs (lncRNAs), which are RNA molecules longer than 200 nucleotides that do not encode proteins, have been recognized as key players in the

Highlight box

Key findings

- The study developed a senescence-related lncRNA signature (SenLncSig) consisting of five long non-coding RNAs (lncRNAs) (AP000695.2, LINC02381, AC005586.1, AP003392.1, and AP001528.2) to predict gastric cancer prognosis. High-risk patients based on this signature had poor overall survival (hazard ratio: 1.498, P<0.001), stronger regulatory T cell and M2 macrophage infiltration, and higher tumor immune dysfunction scores. High tumor mutation burden (TMB) in high-risk patients further worsened prognosis. Quantitative reverse-transcription polymerase chain reaction validated the higher expression of AP000695.2 and AP003392.1 in tumor tissues and lower expression of LINC02381.

What is known and what is new?

- LncRNAs have been suggested as biomarkers for predicting cancer prognosis, and cellular senescence is emerging as a key cancer marker.
- This study introduces a specific lncRNA signature linked to cellular senescence for gastric cancer prognosis, showing that immune microenvironment factors and TMB significantly influence patient outcomes.

What is the implication, and what should change now?

- The findings suggest that SenLncSig can improve patient stratification for prognostic predictions and immunotherapy. Clinicians may need to incorporate this signature into treatment planning, particularly for identifying patients who might benefit from immune-based therapies. Further research on targeting senescence-associated pathways and immune modulation in high-risk gastric cancer patients is warranted.

initiation and progression of various cancers, including GC (11). A recent study reported that the expression levels of lncRNAs changed significantly during the senescence process (12). In addition, research has shown that the silencing of the lncRNA SNHG6 induced the cellular senescence of GC cells by upregulating P21, thereby inhibiting tumor development in mice (13). Research has also shown that lncRNAs could serve as prognostic or diagnostic indicators due to their extensive involvement in gene regulation networks (14,15).

Recent studies have developed various prognostic prediction models for GC, incorporating both genetic signatures and clinical factors to improve patient outcomes. Here are some key findings: $CD8^+$ T cell signature in the TME: A model based on $CD8^+$ T cells identified in GC has shown potential for predicting patient outcomes. This approach aims to integrate immune-related markers in the TME, offering insight into both prognosis and potential immunotherapy responses (16). m6A-related classification: Another study developed a classification and risk signature based on m6A RNA modifications, which revealed the potential to predict prognosis and assess immunotherapy sensitivity. This model highlights the role of RNA modifications in GC and their relationship with patient outcomes (17). A third model based on complement-related gene expression was developed to predict GC prognosis. This model provides a new biomarker target, emphasizing the role of the immune system in cancer progression (18). A model using lncRNA pairs associated with epithelial-mesenchymal transition (EMT) showed promise for prognosis prediction. The role of EMT in GC has been linked to tumor metastasis and immune evasion, making this model highly relevant for personalized treatment plans (19). These models are highly dependent on biological factors such as immune markers (e.g., $CD8^+$ T cells, m6A modifications, and EMT-related markers) and complement genes, which reflect the complex interplay between cancer progression and the immune microenvironment. While these models offer promising tools, they have limitations in terms of generalizability and accuracy due to variations in patient populations, tumor heterogeneity, and treatment regimens. Furthermore, many models still require external validation before widespread clinical adoption. Given these challenges, there is a clear clinical need for new prognostic models that can more accurately predict treatment responses, particularly in the context of immunotherapy. Integrating multiple biological layers, such as immune cell signatures and RNA modifications, alongside clinical features, could significantly improve patient stratification and therapeutic decision-making. Future models should aim for better validation in diverse cohorts to confirm their predictive power and clinical relevance.

We hypothesized that senescence-related lncRNAs are correlated with the prognosis of GC patients. To test this hypothesis, we developed a senescence-related lncRNA signature (SenLncSig) and conducted a comprehensive investigation to explore the association between this signature and GC prognosis. A SenLncSig stratification analysis was conducted to compare the immune cell infiltration status, immune function activation, mutation status, and sensitivity to chemotherapeutic agents, targeted therapy, and immune checkpoint blockades of different GC cohorts. Finally, the expression levels of the three lncRNAs of the model were validated using quantitative reverse-transcription polymerase chain reaction (qRT-PCR) assays in GC cell lines and an independent GC cohort. We present this article in accordance with the TRIPOD reporting checklist (available at https://jgo.amegroups.com/article/view/10.21037/jgo-24-792/rc).

Methods

Data acquisition

We obtained the RNA sequencing data and clinical parameters of GC patients from TCGA-STAD data set (https://portal.gdc.cancer.gov/). The initial phase of the study included 407 GC patients. After excluding patients who lacked complete information and those who survived less than 30 days, 334 patients were finally enrolled in the study. The 279 cellular senescence genes were obtained from the CellAge database (https://genomics.senescence.info/), a collection of genes that regulate cellular senescence, after a manual search of genetic manipulation experiments in the literature (16).

Analysis of the functional enrichment of the senescence-related differentially expressed genes (DEGs) in GC and normal tissues

The R package "limma" was used to identify cellular senescence-related DEGs between the tumor and normal tissues. The DEGs were defined as those DEGs with a false discovery rate (FDR) <0.05 and log fold change (FC) >1 in absolute value. Next, the DEGs were subjected to Gene

Ontology (GO) and Kyoto Encyclopedia of Genes and Genomes (KEGG) analyses.

Construction of the SenLncSig

Using the senescence-related DEGs as the reference gene set and a threshold of a Pearson correlation coefficient absolute value >0.3 and a P value <0.001, we constructed a messenger RNA (mRNA)-lncRNA co-expression network to identify potential lncRNAs. Cytoscape 3.7.2 was used to visualize this network. We generated the co-expressed Sankey diagram using the "ggalluvial" package in R. We then performed a univariate Cox regression analysis to identify the lncRNAs that were significantly associated with prognosis. These lncRNAs were subsequently included in a multifactorial stepwise regression equation to establish the final risk formula and its corresponding regression coefficients.

The risk equation is expressed as follows: risk score = expression levels of lncRNA-1 × coefficient of lncRNA-1 + expression levels of lncRNA-2 × coefficient of lncRNA-2 + … + expression levels of lncRNA-i × coefficient of lncRNA-i. Patients were stratified into high- and low-risk groups based on their risk scores, with the median risk score serving as the threshold. We named this lncRNA predictive signature the SenLncSig. The survival status of each patient was investigated according to the risk-score level. The clinicopathological data were analyzed using univariate and multivariate Cox regression analyses to determine whether the SenLncSig risk score was an independent prognostic indicator. The receiver operating characteristic (ROC) curve was used to assess the accuracy of the risk model. We used the "pheatmap" and "scatterplot3d" packages in R to create and illustrate the clinicopathological variables and principal component distributions of the distinct risk groups, respectively.

Internal validation of the SenLncSig

The TCGA-STAD cohort, comprising 334 GC patients, was randomly divided into two internal validation cohorts (168 and 166 patients, respectively) to rigorously evaluate the accuracy of the SenLncSig model. Overall survival (OS) data, measured in months from diagnosis to death or last follow-up, served as the primary outcome. Survival probabilities at 1-, 3-, and 5-year intervals were calculated, and time-dependent ROC curves were generated to verify the model's predictive efficacy. Baseline clinical factors included demographic data (age, gender), pathological features (tumor grade, TNM stage), and molecular signatures (SenLncSig risk scores based on five senescence-related lncRNAs). These factors were utilized to validate the model's robustness and reliability for prognostic prediction.

Nomograph construction

We constructed a nomograph that predicted 1-, 3-, and 5-year survival in GC patients by combining risk scores with clinicopathological features, such as age, sex, tumor (T) stage, and Node (N) stage. The nomograph was created and validated in R using the "rms" package.

Gene set enrichment analysis (GSEA)

The biological pathways in the different risk groups were visualized using a GSEA and the ggplot2 package with a nominal (NOM) P value <0.05 and a FDR q value <0.25.

Tumor mutation burden (TMB) analysis

We obtained information on somatic alterations in GC patients from the TCGA-STAD data set. Next, the number of non-synonymous point mutations was calculated for each sample using the "maftools" package (17). Finally, survival curves were plotted based on the TMB and risk score stratification.

Estimation of immune cell infiltration

A single-sample gene set enrichment analysis (ssGSEA) was conducted to calculate the infiltrating fraction of 16 immune cells and the activity of 13 immune-related functions (18). We also used the CIBERSORT algorithm to cross-reference the results with those of the ssGSEA (19).

Potential clinical drug treatment option from the predictive signature

First, we compared the expression levels of 47 immune checkpoint genes across the different risk groups. Responses to anti-PD-1 and anti-CTLA4 immunotherapies were distinguished by tumor immune dysfunction and immune exclusion (TIDE) modules (http://tide.dfci.harvard.edu/). Moreover, we employed the "pRRophetic" software package to quantitatively compare the half-maximal inhibitory concentration (IC_{50}) values of commonly used drugs,

Table 1 Clinical characteristics of the quantitative reverse-transcription polymerase chain reaction independent validation GC group (n=30)

Characteristics	N (%)
Age (years)	
Median	64.2
Range	37–80
Gender	
Female	11 (36.67)
Male	19 (63.33)
Tumor location	
Corpus	11 (36.67)
Antral	15 (50.00)
Cardia	4 (13.33)
Disease stage	
I	3 (10.00)
II	9 (30.00)
III	18 (60.00)
T stage	
T1	2 (6.67)
T2	2 (6.67)
T3	24 (80.00)
T4	2 (6.67)
N stage	
N0	10 (33.33)
N1	2 (6.67)
N2	9 (30.00)
N3	9 (30.00)
Histological appearance	
Well	9 (30.00)
Well to moderately	7 (23.33)
Moderately	10 (33.33)
Poorly	4 (13.33)

GC, gastric cancer; T, extension of the primary tumor; N, lymph node invasion.

to evaluate whether the developed model could predict sensitivity to chemotherapy and targeted therapies.

Independent validation sample recruitment

Pathological evidence of GC in the patients enrolled was required in this study. The American Joint Committee on Cancer 8th edition was used for tumor staging (20). The main exclusion criteria included: stage IV and the use of any systemic or local anti-cancer treatment prior to surgery. *Table 1* displays the baseline demographic and clinical characteristics of the GC group as assessed through a qRT-PCR-independent validation analysis.

Tissue samples were collected from patients with pathologically confirmed gastric adenocarcinoma at The Sixth Affiliated Hospital of Sun Yat-sen University between 2020 and 2021. None of these patients received preoperative chemotherapy, targeted therapy, immunotherapy, or radiotherapy. Tumor tissue samples and adjacent non-tumor tissues (5 cm from the tumor edge) were stored in RNAfixer reagent (Bioteke, Beijing, China). The study was conducted in accordance with the Declaration of Helsinki (as revised in 2013). This study was authorized by the Research Ethics Committee of The Sixth Affiliated Hospital of Sun Yat-sen University (protocol code: 2020ZSLYEC-284). Written informed consent was obtained from all the participants.

Cell culture and qRT-PCR

We purchased three human GC cell lines (MKN45, HGC27, and AGS) and one human normal gastric mucosal cell line (GES1) from the Type Culture Collection Cell Bank of the Chinese Academy of Sciences Committee (Shanghai, China). The AGS cell line was cultured in DMEM/F12, while the other cell lines were cultured in RPMI 1640 medium. The cells were incubated at 37 ℃ in a humid environment with 5% carbon dioxide, and all the media contained 1% penicillin-streptomycin and 10% fetal bovine serum from Invitrogen (CA, USA).

Total RNA from cell lines or specimen tissues was extracted using TRIzol reagent (Invitrogen) and the RNA-Quick Purification Kit (ES-RN001; Yishan Biotechnology, Shanghai, China). Reverse-transcription polymerase chain

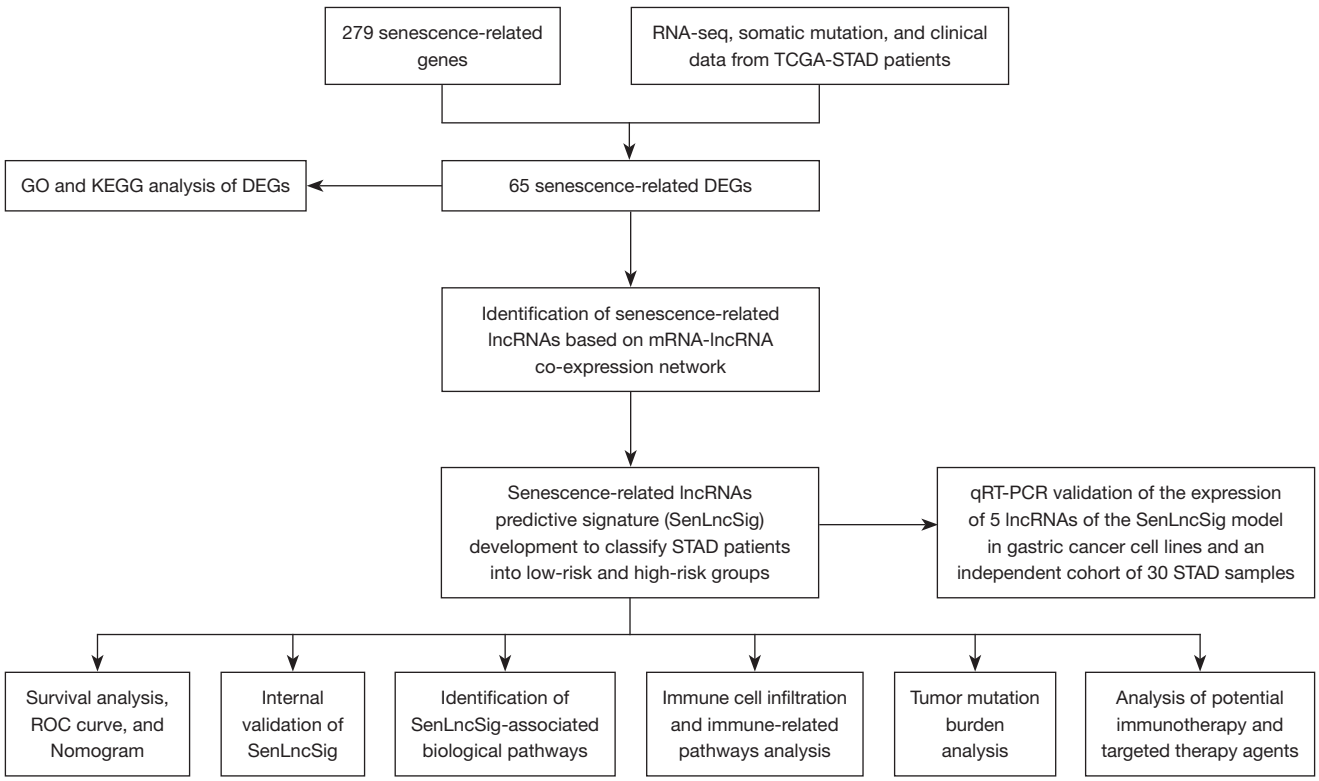

Figure 1 Flow chart of the present study. RNA-seq, RNA sequence; TCGA-STAD, The Cancer Genome Atlas-stomach adenocarcinoma; DEG, differentially expressed gene; GO, Gene Ontology; KEGG, Kyoto Encyclopedia of Genes and Genomes; mRNA, messenger RNA; lncRNA, long non-coding RNA; qRT-PCR, quantitative real-time polymerase chain reaction; ROC, receiver operating characteristic.

reaction (RT-PCR) and quantitative real-time polymerase chain reaction were performed as previously described (21). *GAPDH* was used as a normalization control. The qRT-PCR primer sequences are listed in Table S1. The relative expression of the genes was compared using the $2^{-\Delta Ct}$ or $2^{-\Delta\Delta Ct}$ method.

Statistical analysis

The expression levels of the cellular senescence-related DEGs in the tumor tissues and normal tissues were compared using the Wilcoxon test. To compare OS between the patients in the high- and low-risk groups, the Kaplan-Meier method and the log-rank test were used. To construct the ROC curves and calculate their corresponding areas under the curve (AUCs), we employed the "survivalROC" package. We validated the accuracy of the SenLncSig model using the "survivalROC" in R, generating time-dependent ROC curves and calculating AUC values for 1-year, 3-year, and 5-year survival predictions. An AUC > 0.7 indicates good predictive performance, while AUC values between 0.5 and 0.7 reflect moderate accuracy. The Kruskal-Wallis test was used to analyze differences between groups. The Chi-squared test or Fisher's exact test was used to analyze the clinical data. We used R software (version 4.1.2) for the statistical analysis of all the results in this research.

Results

Enrichment analysis of senescence-related DEGs in GC

Figure 1 presents a flow chart of this study. A total of 279 senescence-related genes (Table S2) were first used to examine their differential expression in the tumor and normal tissues. A total of 65 DEGs were obtained, of which 28 were downregulated, and 37 were upregulated in the GC tumor tissues (*Figure 2A*,*2B*, Table S3). The results of the functional enrichment analysis suggested that the five most abundant KEGG pathways were the p53 signaling pathway, cellular senescence, cell cycle, human T-cell leukemia virus 1 infection, and oocyte meiosis (*Figure 2C*); while the five

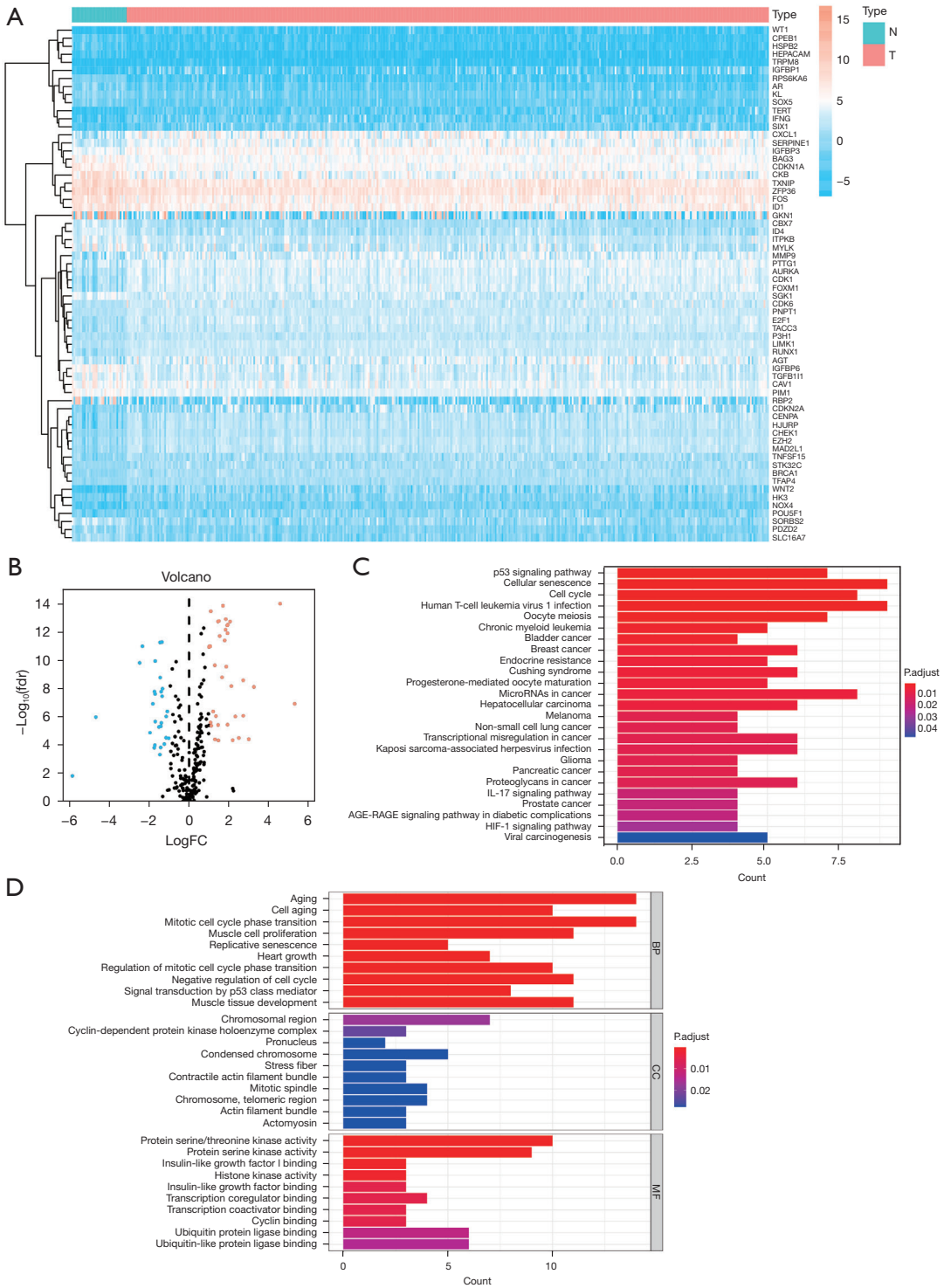

Figure 2 Detection and enrichment analysis of senescence-related DEGs. (A) Heat map showing senescence-related DEGs (n=65) in GC tissues and para-cancer tissues. (B) Sixty-five DEGs were mapped in volcanoes of normal and GC tumor tissues. The pink dots represent the upregulated DEGs; the blue dots represent the downregulated DEGs, and the black dots indicate DEGs without significant differential expression. (C) KEGG functional enrichment analysis of the 65 DEGs. (D) GO functional enrichment analysis of the 65 DEGs. DEGs, differentially expressed genes; GC, gastric cancer; N, normal tissue; T, tumor tissue; FC, fold change; KEGG, Kyoto Encyclopedia of Genes and Genomes; GO, Gene Ontology; FDR, false discovery rate; BP, biological process; CC, cellular component; MF, molecular function.

most abundant GO term categories were aging, cell aging, mitotic cell cycle phase transition, muscle cell proliferation, and replicative senescence (*Figure 2D*).

Development of the SenLncSig

Strong correlations were found between the 65 senescence-related DEGs and 729 lncRNAs (the supplementary table is available at: https://cdn.amegroups.cn/static/public/jgo-24-792-1.xlsx). Using a univariate Cox regression analysis, we found that 18 of the 729 lncRNAs were significantly associated with GC prognosis (*Figure 3A*). Based on the analysis of a multivariate Cox regression model, five lncRNAs (i.e., AP000695.2, LINC02381, AC005586.1, AP003392.1, and AP001528.2) were included in the SenLncSig. *Figure 3B* shows the expression profile of these SenLncSig lncRNAs in GC patients. Finally, the network of the co-expressed lncRNAs and mRNAs relevant to senescence was displayed using Cytoscape software (*Figure 3C*) and Sankey plots (*Figure 3D*).

The ability of the SenLncSig to predict the prognosis of GC patients

The risk score formula for the SenLncSig comprised six lncRNA expression levels and coefficients. The formula used to calculate the SenLncSig risk score is expressed as follows: SenLncSig risk score = (0.42828251 × AP000695.2 expression) + (0.165666613 × LINC02381 expression) + (–0.452677374 × AC005586.1 expression) + (–0.877187333 × AP003392.1 expression) + (0.602786873 × AP001528.2 expression). After calculating the individual risk score for each patient, we combined the scores, and divided the patients into two categories based on the median value. Of the total cohort, 172 cases were allocated to the high-risk group, and 162 cases were allocated to the low-risk group (*Figure 4A*). A Kaplan-Meier analysis demonstrated that the patients in the high-risk group had a significantly shorter OS time than those in the low-risk group (*Figure 4A*). The risk score and survival statistics for each patient are shown in *Figure 4B,4C*. Further, as *Figure 4D,4E* show, the risk score was found to be an independent prognostic factor for patients with GC. Compared to the other clinical parameters, such as age (AUC =0.636) and disease stage (AUC =0.575), the SenLncSig risk-score model had an AUC of 0.711, and thus had a superior ability to predict the prognosis of GC patients (*Figure 4F*). In addition, the time-dependent ROC curves demonstrating the AUCs at 1-, 3- and 5-year (of 0.661, 0.698 and 0.68, respectively) also showed the good performance of the model (*Figure 4G*).

Figure 5A depicts the correlations between the SenLncSig model and clinical parameters. To differentiate between the high- and low-risk patients, we conducted a principal component analysis (PCA) with whole-genome, senescence-related DEGs, senescence-related lncRNAs, and the SenLncSig (*Figure 5B-5E*). In contrast to the other models, only the SenLncSig (*Figure 5E*) could distinguish between the low- and high-risk groups.

We further conducted a Kaplan-Meier survival analysis to compare the survival rates of the patients stratified by various clinicopathological variables (*Figure 6A-6U*). When stratified by age (*Figure 6A,6B*), sex (*Figure 6C,6D*), grades 2 and 3 (*Figure 6F,6G*), stage M0 (*Figure 6H*), stage N (N0–N3) (*Figure 6J-6M*), stages 2 and 3 (*Figure 6O,6P*), and stages T3 and T4 (*Figure 6T,6U*), the SenLncSig risk score was also able to distinguish between patients the high-risk group from the low-risk group in terms of OS.

Nomograph development

We developed a clinically adaptable nomograph based on the SenLncSig risk score and other clinicopathological factors to estimate the 1-, 3-, and 5-year survival probabilities of patients with GC (*Figure 7A*). The calibration plots for 1-, 3-, and 5-year survival also showed the accuracy of the nomograph (*Figure 7B-7D*).

Internal validation of the SenLncSig

To test the ability of the SenLncSig to predict the OS of GC patients, we randomly divided the entire 334 TCGA-STAD cohort into two cohorts (with n=168 in the first internal cohort, and n=166 in the second internal cohort, *Figure 8A-8D*). As *Figure 8A,8C* show, patients in the high-risk group had lower OS than those in the low-risk group in both the first and second cohorts. This finding is consistent with the results obtained from the entire TCGA-STAD data set. Further, the time-dependent ROC curves also indicated the good efficacy of the model. In the first internal cohort, the AUCs for 1-, 3-, and 5-year survival were 0.701, 0.687, and 0.734, respectively (*Figure 8B*), while in the second internal cohort, the AUCs were 0.629, 0.736, and 0.679, respectively (*Figure 8D*). We confirmed the robust ability of the SenLncSig to predict the prognosis of GC patients using internal validation cohorts.

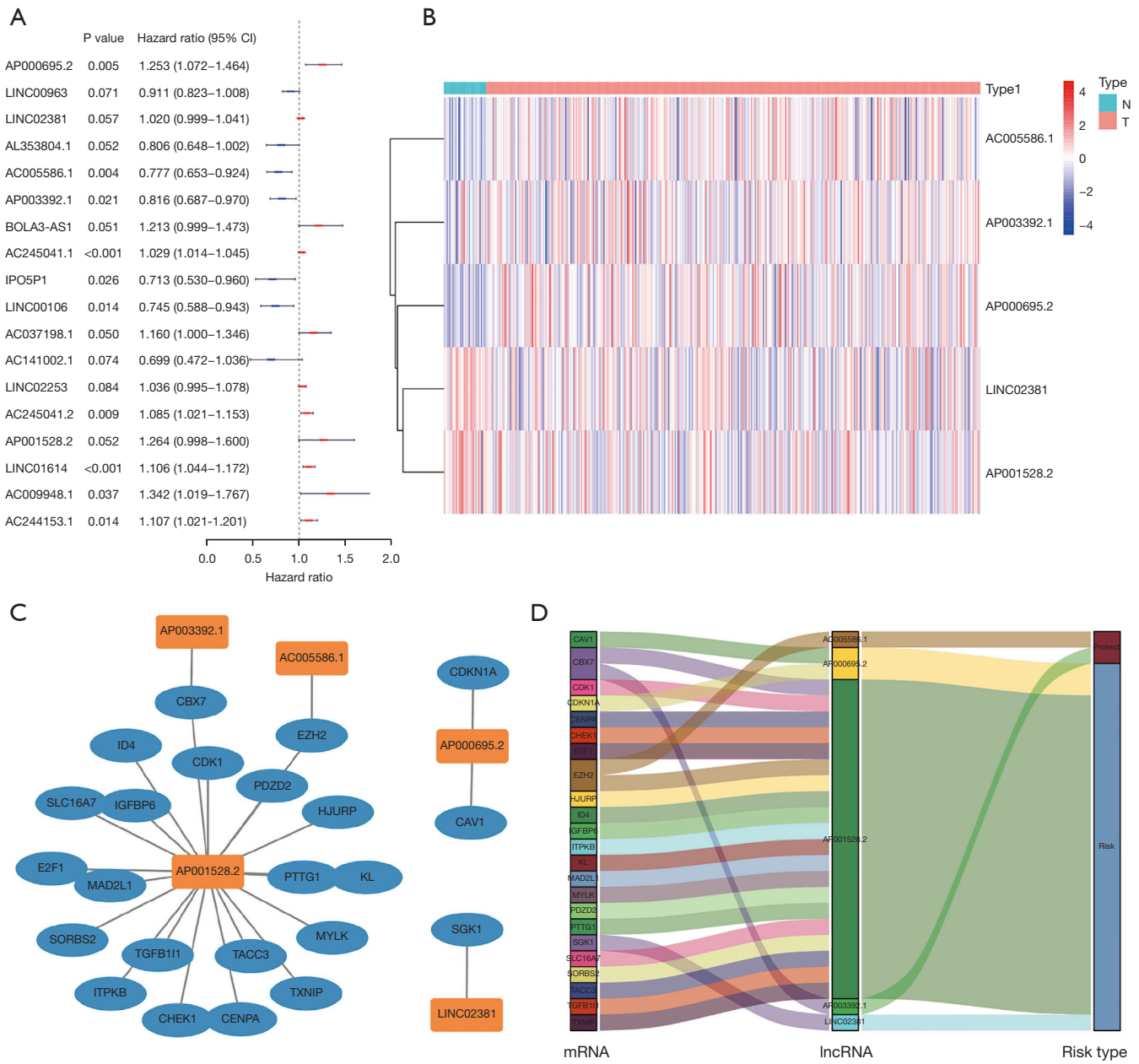

Figure 3 The identification of senescence-related lncRNAs linked to GC prognosis, and the construction of a lncRNA-mRNA co-expression network. (A) Forest plots of 18 lncRNAs with their associated P values for GC prognosis, univariate Cox proportional hazards analysis hazard ratios, and 95% confidence intervals. (B) Heat map showing multivariate Cox regression analysis results for the expression levels of the five senescence-related lncRNAs linked to GC prognosis. The lncRNA-mRNA co-expression network is shown in Figure (C). Prognostic lncRNAs are represented by orange squares; senescence-related mRNAs are represented by blue ovals. In total, 23 senescence-related mRNA levels and the expression levels of five senescence-associated lncRNAs were connected. (D) Sankey plots displaying the relationship between risk type and prognostic senescence-related lncRNAs and mRNAs. P<0.1 indicates statistical significance. lncRNAs, long non-coding RNAs; GC, gastric cancer; mRNAs, messenger RNAs; N, normal tissue; T, tumor tissue.

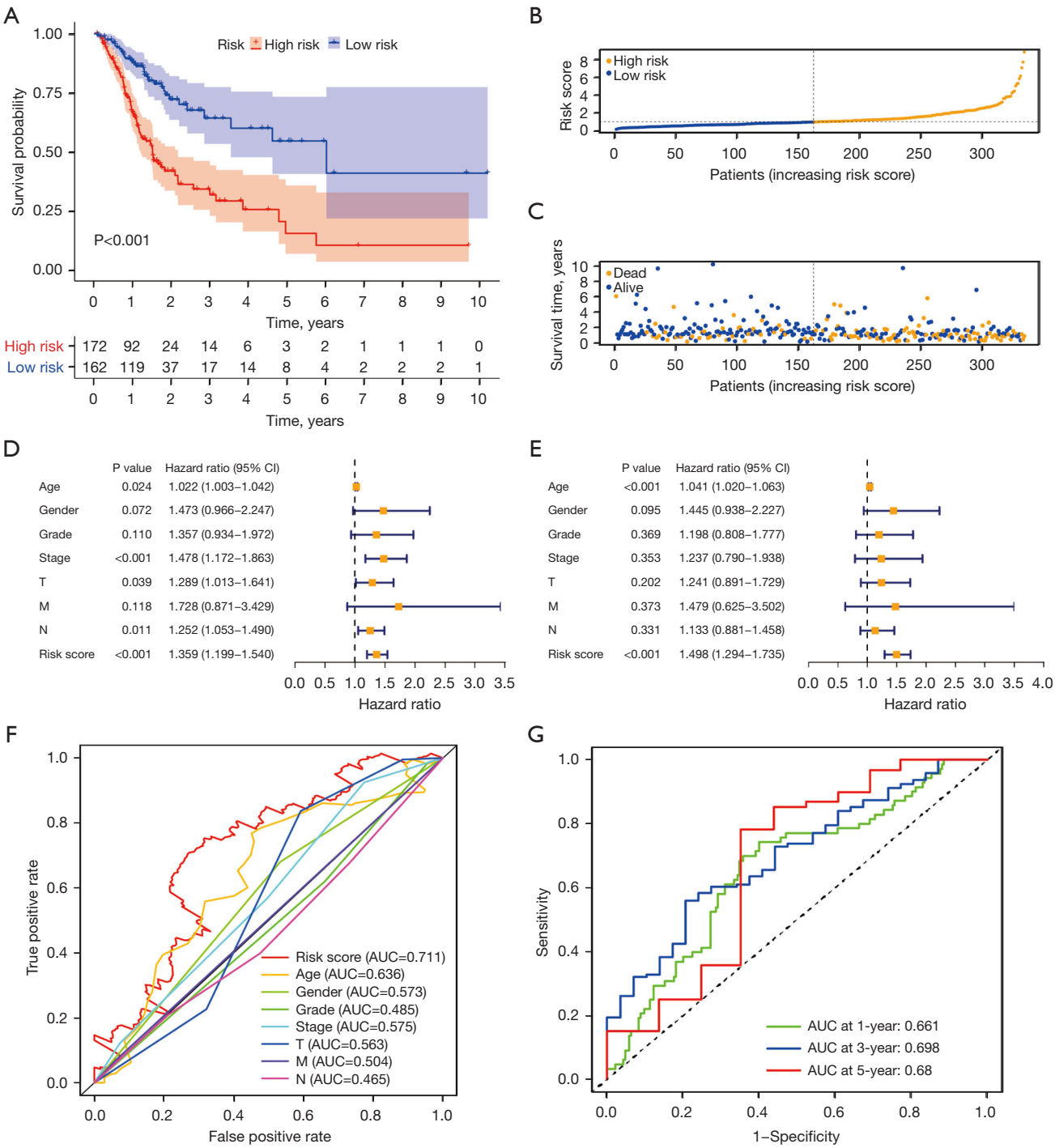

Figure 4 Prognostic value of the risk score of the SenLncSig model. (A) SenLncSig median risk score–based Kaplan-Meier curves for OS in the high- and low-risk groups. (B) A risk curve based on the risk score for each sample; the orange dots denote high risk; the blue dots denote low risk. (C) A scatter plot was constructed based on the survival status of each sample; the orange and blue dots represent death and survival, respectively. Forest plots of univariate Cox regression analysis (D) and multivariate Cox regression analysis (E) demonstrate that risk score is a significant prognostic parameter. (F) According to the ROC curves, risk scores and other clinicopathological factors had prognostic significance. (G) Time-dependent ROC curves showing the ability of the signature to predict 1-, 3-, and 5-year survival. SenLncSig, senescence-related lncRNA signature; OS, overall survival; ROC, receiver operating characteristic; AUC, area under the curve; T, tumor; M, distant metastasis; N, lymph node metastasis.

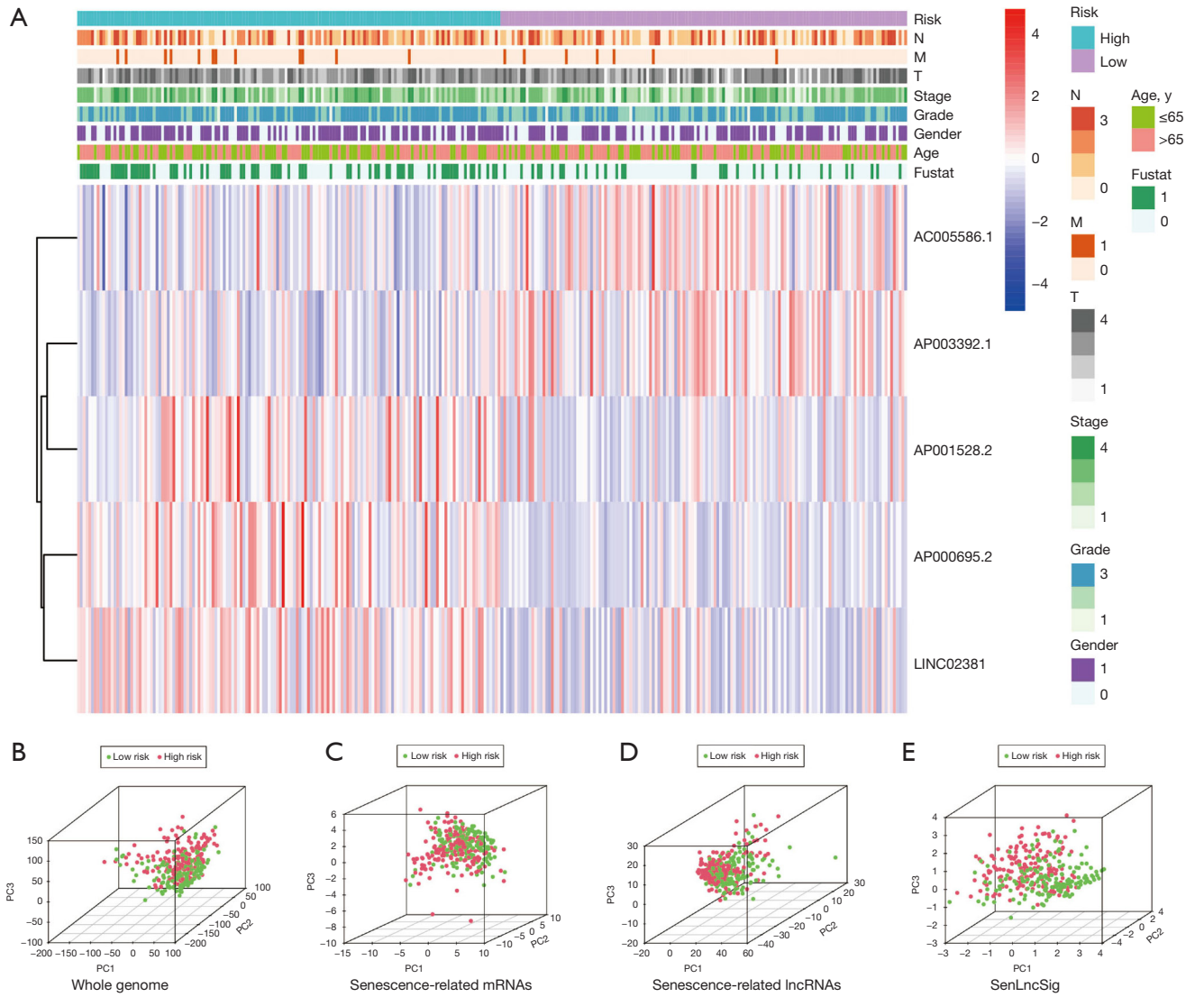

Figure 5 Using clinicopathological variable stratification and conducting a PCA of the gene sets, the patients were classified into different risk groups based on the expression levels of five prognostic lncRNAs related to senescence. (A) A heat map was constructed for the high- and low-risk groups, displaying the expression levels of the five prognostic senescence-related lncRNAs along with the clinicopathological variables. A PCA was performed on the gene expression of (B) whole-genome mRNA transcripts, (C) senescence-related differentially expressed mRNAs, (D) senescence-related lncRNAs, and (E) a risk model comprising the five SenLncSig senescence-related lncRNAs. Patients with high-risk scores are represented in red, while those with low-risk scores are represented in green. PCA, principal component analysis; lncRNAs, long non-coding RNAs; mRNA, messenger RNA; T, tumor; N, lymph node metastasis; M, distant metastasis; SenLncSig, senescence-related lncRNA signature.

GSEA

We used GSEA software for the gene function annotation of both the high-risk and low-risk GC patients. In the high-risk group, the enriched KEGG pathways included the extracellular matrix (ECM) receptor interaction [normalized enrichment score (NES) =2.14, NOM P<0.001, FDR q=0.029], hypertrophic cardiomyopathy (NES =2.12, NOM P<0.001, FDR q=0.016), complement and coagulation cascades (NES =2.07, NOM P<0.001, FDR q=0.022), glycosaminoglycan degradation (NES =2.05, NOM P<0.001, FDR q=0.02), dilated cardiomyopathy (NES =1.99, NOM P<0.001, FDR q=0.034), prion diseases (NES

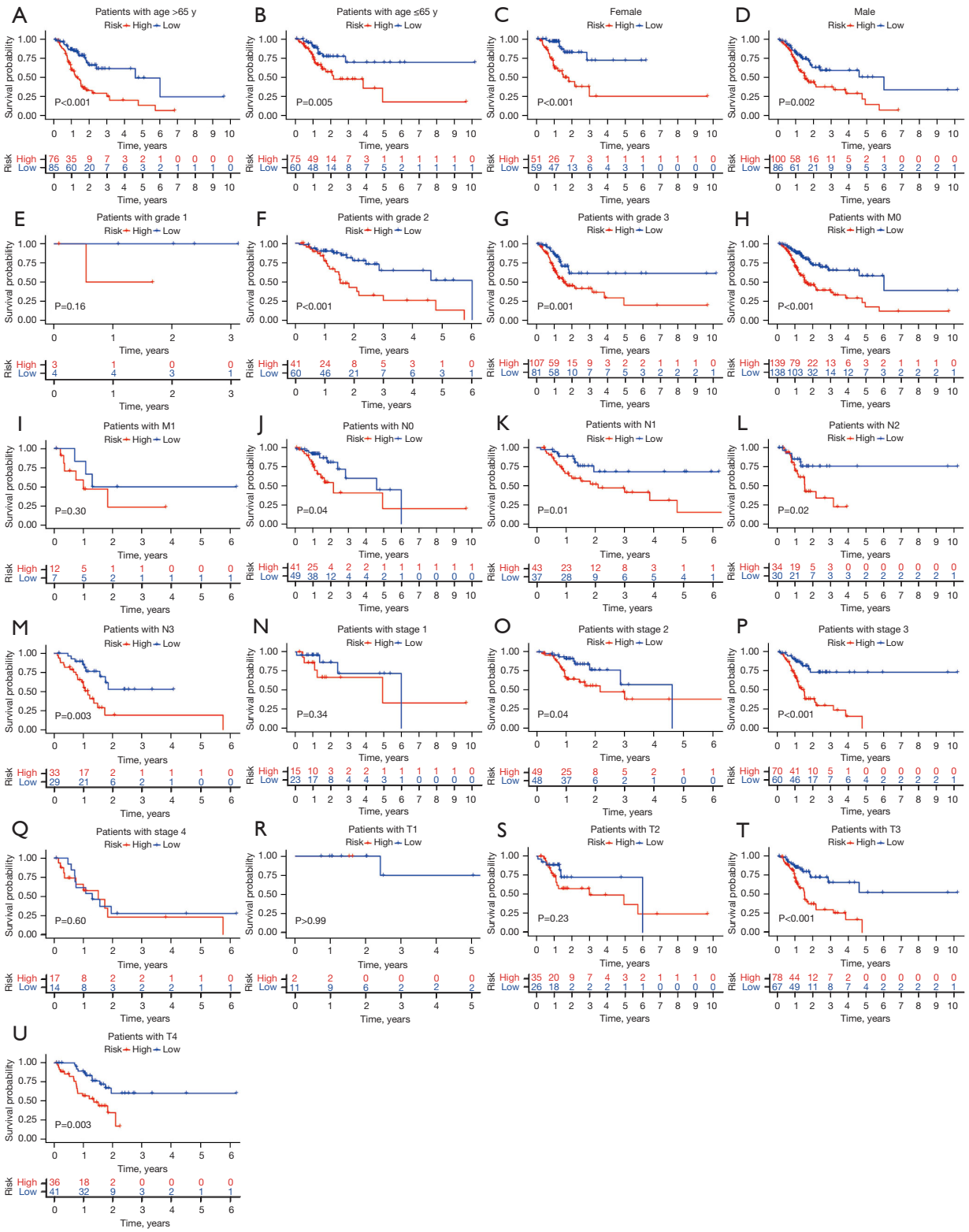

Figure 6 Kaplan-Meier survival curves were generated to compare the survival rates of the high- and low-risk patient groups sorted by clinicopathological variables. The variables analyzed included (A,B) age, (C,D) sex, (E-G) grade, (H,I) M stage, (J-M) N stage, (N-Q) overall stage, and (R-U) T stage. T, tumor; N, lymph node metastasis; M, distant metastasis.

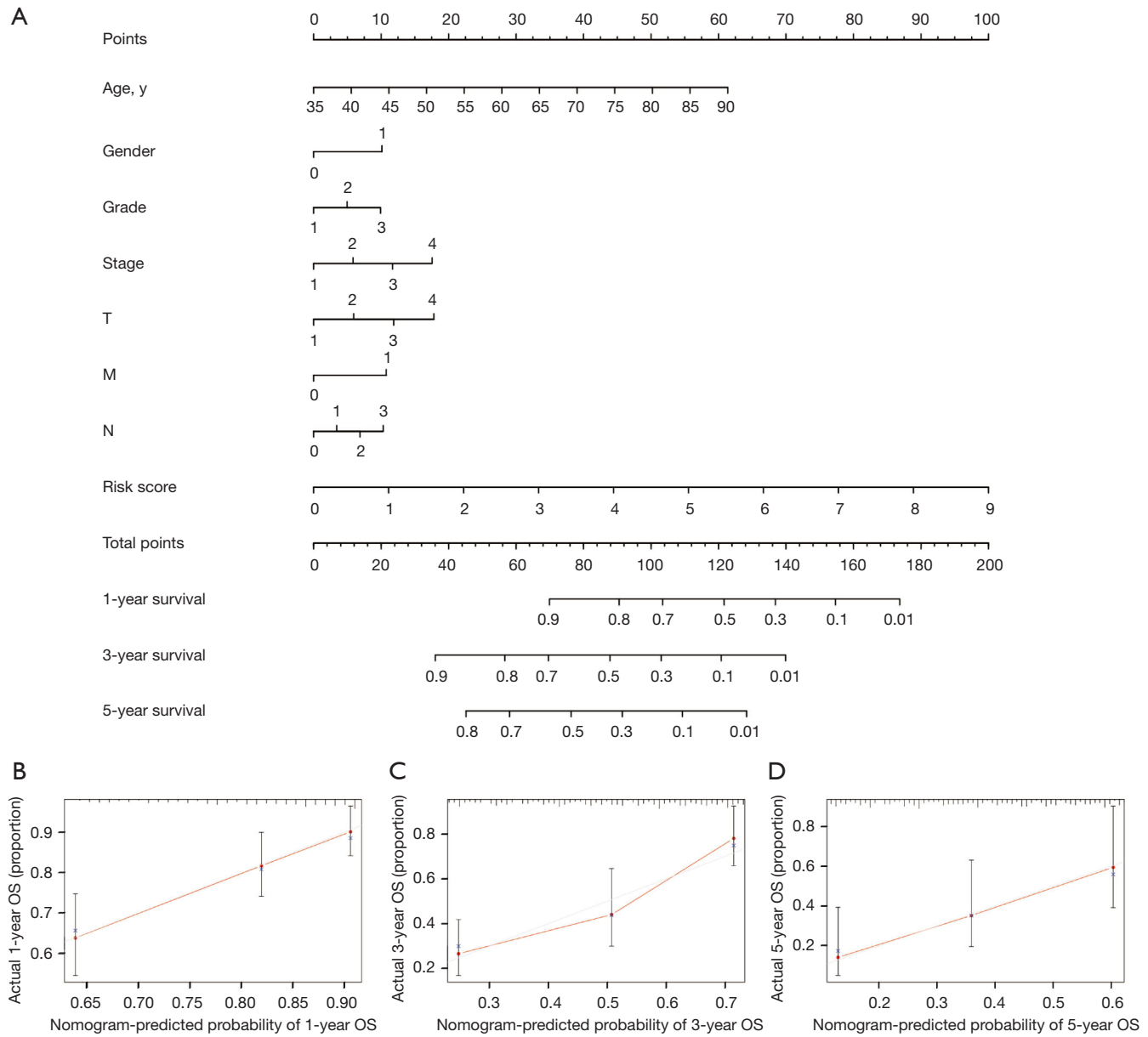

Figure 7 A nomogram was created and validated that combined clinicopathological variables and risk scores to predict the 1-, 3-, and 5-year survival probabilities of patients with gastric cancer. (A) The nomogram consists of a graph with axes representing various clinical factors, and the corresponding numerical values assigned based on their respective contributions to the OS prediction. Calibration curves were plotted to evaluate the concordance between the predicted and actual OS at (B) 1, (C) 3, and (D) 5 years. OS, overall survival; T, tumor; N, lymph node metastasis; M, distant metastasis.

=1.97, NOM P<0.001, FDR q=0.037), glycosaminoglycan biosynthesis chondroitin sulfate (NES =1.96, NOM P<0.001, FDR q=0.033), cell adhesion molecules (NES =1.89, NOM P=0.009, FDR q=0.06), neuroactive ligand receptor interaction (NES =1.88, NOM P=0.002, FDR q=0.054), and glycosphingolipid biosynthesis-ganglio series (NES =1.88, NOM P=0.004, FDR q=0.051) (*Figure 9A*). The gene sets enriched in the low-risk group did not reach the FDR q<0.25 threshold. Conversely, in the high-risk group, the GO terms enriched in the GC patients included

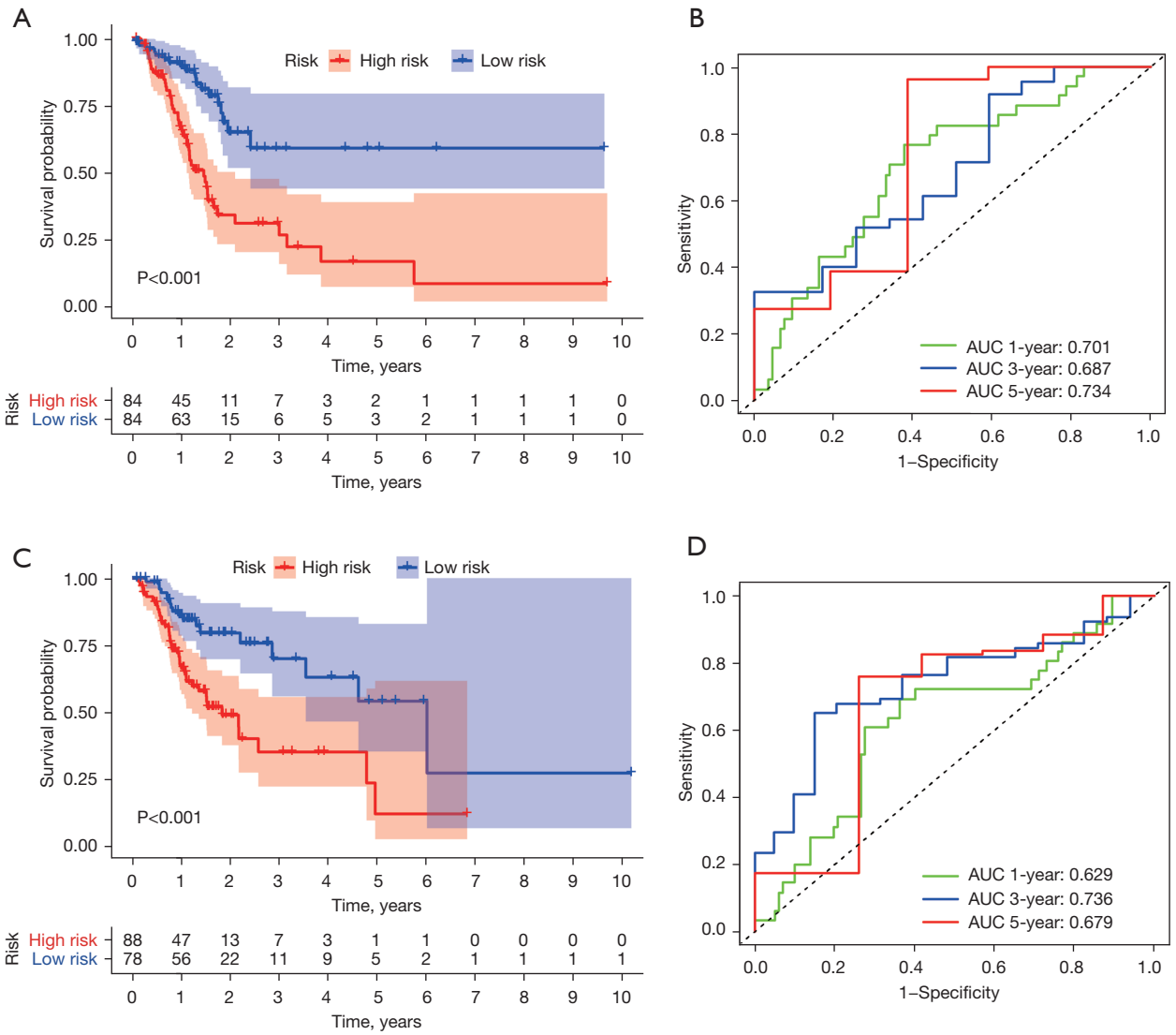

Figure 8 Internal validation of the SenLncSig model for OS was performed using two internal cohorts. To assess the performance of the SenLncSig model for predicting OS in the first internal cohort, Kaplan-Meier survival curves were plotted in (A). ROC curve and AUC values were calculated for 1-, 3-, and 5-year survival in the same cohort as presented in (B). To evaluate the predictive ability of the SenLncSig model in terms of OS in the second internal cohort, Kaplan-Meier survival curves were plotted in (C). Further, ROC curves and AUC values were calculated for 1-, 3-, and 5-year survival in the same cohort as presented in (D), similar to the first internal cohort. P<0.05 indicates statistical significance. SenLncSig, senescence-related lncRNA signature; OS, overall survival; ROC, receiver operating characteristic; AUC, area under the curve.

collagen-containing ECM (NES =2.51, NOM P<0.001, FDR q<0.001), ECM structural constituent (NES =2.44, NOM P<0.002, FDR q<0.001), basement membrane (NES =2.43, NOM P<0.003, FDR q<0.001), growth factor binding (NES =2.39, NOM P<0.004, FDR q<0.001), and glycosaminoglycan binding (NES =2.35, NOM P<0.005, FDR q<0.001, *Figure 9B*). In the low-risk group, the gene sets did not reach the FDR q<0.25 threshold for enriched terms.

The relationship between the SenLncSig risk scores and somatic mutations and the TMB

We investigated the differences in the TMB between

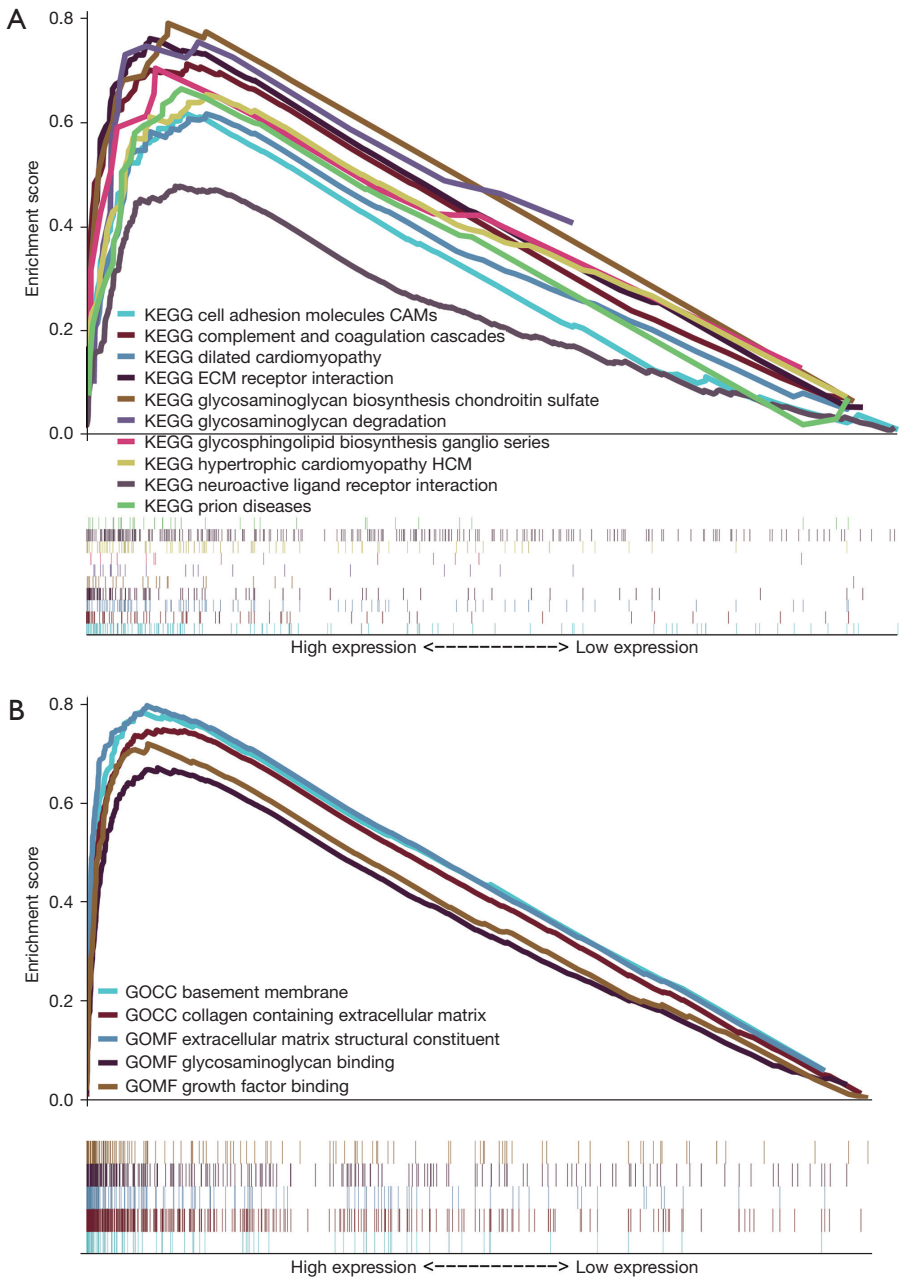

Figure 9 A GSEA was performed on the different risk groups based on the SenLncSig. The GSEA results showed that senescence-related lncRNA expression differentially enriched KEGG genes as presented in (A). Ten KEGG items (i.e., ECM receptor interaction, hypertrophic cardiomyopathy, complement and coagulation cascades, glycosaminoglycan degradation, dilated cardiomyopathy, prion diseases, glycosaminoglycan biosynthesis chondroitin sulfate, cell adhesion molecules, neuroactive ligand receptor interaction, and glycosphingolipid biosynthesis-ganglio series) were enriched in the high-risk group based on the NES, NOM P value, and FDR value. (B) The SenLncSig-based GSEA also revealed significantly enriched DEGs in GO pathways (the five GO items were: collagen-containing ECM, ECM structural constituent, basement membrane, growth factor binding, and glycosaminoglycan binding) associated with the senescence-related lncRNAs. The high-expression phenotype showed greater differential enrichment based on the NES, NOM P value, and FDR value. GSEA, Gene Set Enrichment Analysis; KEGG, Kyoto Encyclopedia of Genes and Genomes; SenLncSig, senescence-related long non-coding RNA signature; ECM, extracellular matrix; NES, normalized enrichment score; NOM, nominal; FDR, false discovery rate; DEGs, differentially expressed genes; GO, Gene Ontology; CC, cellular component; MF, molecular function.

the low- and high-risk GC patients. The landscape of somatic variation depicts the mutation patterns of the top 15 driver genes that changed the most frequently (*Figure 10A,10B*). *TTN* (60% *vs.* 41%), *TP53* (45% *vs.* 40%), *MUC16* (34% *vs.* 26%), and the other 12 genes had higher somatic mutation rates in the low-risk group than the high-risk group. The TMB levels were also significantly higher in the low-risk group than the high-risk group (*Figure 10C*). A high TMB level appears to benefit GC patients, as it was associated with a significantly prolonged survival time (log-rank test P=0.02, *Figure 10D*). In addition, patients in the low-risk group who also had a high TMB had an even better prognosis than other groups (*Figure 10E*). Our results provide novel insights into the intrinsic relationship between senescence and somatic variation in GC.

The association between the SenLncSig risk scores and immune infiltration

The ssGSEA algorithm showed that the number of activated dendritic cells (aDCs), B cells, DCs, immature dendritic cells (iDCs), macrophages, mast cells, neutrophils, NK cells, plasmacytoid dendritic cells (pDCs), T helper cells, tumor-infiltrating lymphocytes (TILs), and Tregs differed significantly between the high- and low-risk groups (*Figure 11A*). Moreover, the immune functions, such as antigen-presenting cell (APC) co-inhibition, APC co-stimulation, C-C chemokine receptor (CCR), checkpoint, human leukocyte antigen (HLA), parainflammation, T-cell co-stimulation, type I interferon (IFN) response, and type II IFN response, also differed significantly between the two groups (*Figure 11B*). To validate the results of the ssGSEA, we used another algorithm to estimate immune cell infiltration in the TME; that is, the CIBERSORT algorithm. We found that the follicular helper T cells (P=0.04), monocytes (P=0.02), M0 macrophages (P=0.001), M2 macrophages (P<0.001), and resting DCs (P<0.001) varied significantly between the high- and low-risk subgroups (*Figure 11C*). The high-risk group had more Tregs (P<0.001, *Figure 11A*) and M2 macrophages (P<0.001, *Figure 11C*) than the low-risk group. This finding could explain why patients in the low-risk group had a better prognosis than those in the high-risk group. These results may be indicative of immune checkpoint inhibitor (ICI) efficacy, as ICI agents need a "hot" immunological microenvironment to function effectively (22).

Potential relationships between the SenLncSig and GC system therapy

We first evaluated the expression of immune checkpoints in the two GC risk subgroups. Immunotherapy markers, such as *CD276* (23) and *PDCD1LG2* (24), which are currently being studied in preclinical trials, were found to be significantly more highly expressed in the high-risk group than the low-risk group (*Figure 12A*). Further, the TIDE program (25) was used to predict the effect of immunotherapy, and as *Figure 12B* shows, we discovered that the high-risk group had higher TIDE scores than the low-risk group. Our findings suggest that the worse prognosis of the high-risk group may be explained by the higher possibility of immunotherapy resistance as indicated by a high TIDE score.

Previous research has demonstrated that a senescent microenvironment can contribute to chemotherapy and targeted treatment resistance (26). Therefore, we assessed the efficacy of chemotherapy and target therapy for GC patients in different risk groups to see if the SenLncSig could assist in guiding these treatments. As *Figure 12C,12D* show, there were significant differences between the high- and low-risk groups for some frequently used chemotherapy drugs for GC, such as docetaxel and doxorubicin. Conversely, as *Figure 12E,12F* show, other drugs, like cisplatin and paclitaxel, did not show significant differences between the two groups. These results suggest the potential utility of our model in guiding personalized medication decisions.

In addition, clinical trials involving GC have so far only developed trastuzumab as a single target for HER2-positive patients. Thus, we investigated the new families of targeted drugs, including tyrosine kinase inhibitors, such as erlotinib (*Figure 12G*) and gefitinib (*Figure 12H*), the hedgehog pathway inhibitor GDC-0449 (*Figure 12I*), and the HSP90 inhibitor AUY922 (*Figure 12J*) to offer alternative treatment options when taking senescence into account. Obviously, these targeted therapy strategies still require extensive preclinical and clinical studies to confirm their efficacy. However, our drug sensitivity assays have the potential to aid in the development of individualized therapy regimens for GC patients.

The expression levels of the five lncRNAs included in the SenLncSig model were evaluated in both GC cell lines and an independent GC cohort

When the lncRNA expression levels in the three GC cell

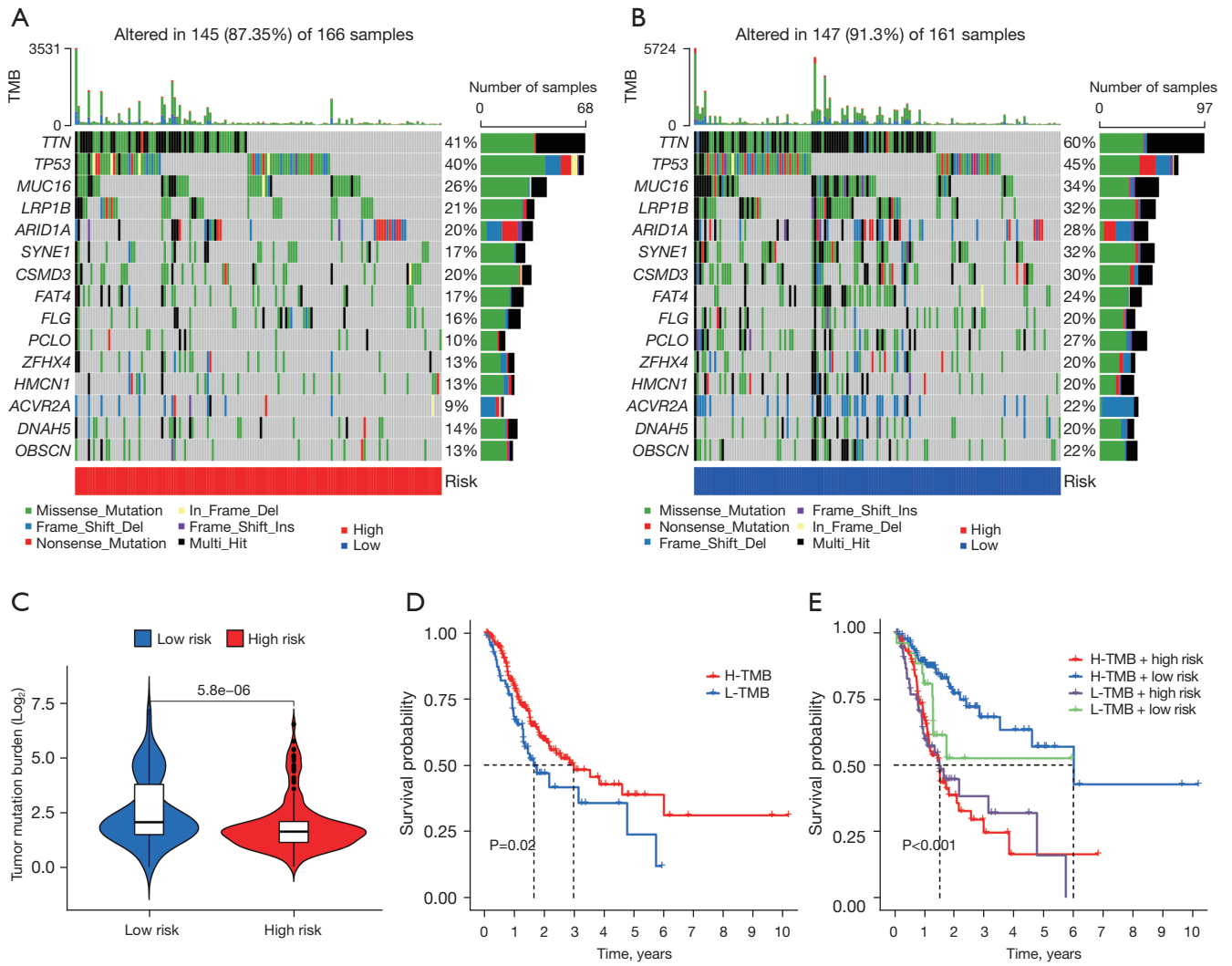

Figure 10 The association between the SenLncSig risk scores, somatic mutations, and TMB. The somatic mutation landscape of the high- and low-risk gastric cancer patients was compared using a waterfall plot as shown in (A) and (B). The difference in the TMB between the low- and high-risk score subgroups is presented in (C), and the Kaplan-Meier curves were plotted for the high- and low-TMB groups in (D). Further, the patients were stratified based on both the TMB and risk scores, and the Kaplan-Meier curves were plotted as shown in (E). The P value represents the result of an analysis of variance between the subgroups. P<0.05 indicates statistical significance. SenLncSig, senescence-related long non-coding RNA signature; TMB, tumor mutation burden.

lines (MKN45, HGC27, and AGS) were compared to those in a human gastric epithelial cell line (GES1), the results revealed that the five lncRNAs exhibited significant differences between the tumor and normal cell lines (*Figure 13A-13E*). AP000695.2 (*Figure 13A*), AP003392.1 (*Figure 13B*), and AC005586.1 (*Figure 13C*) were found to have a significantly higher expression level in the tumor tissues than the normal tissues, while LINC02381 (*Figure 13D*) and AP001528.2 (*Figure 13E*) exhibited the opposite pattern.

To independently validate the expression levels of the lncRNAs included in the SenLncSig model, an external cohort of 30 pairs of tumor and non-tumor tissues from the GC patients was included (*Figure 13F-13J*). AP000695.2 (*Figure 13F*) and AP003392.1 (*Figure 13G*) were found to have significantly higher expression levels in the tumor tissues than the normal tissues, while LINC02381 (*Figure 13I*) exhibited the opposite pattern. The expression

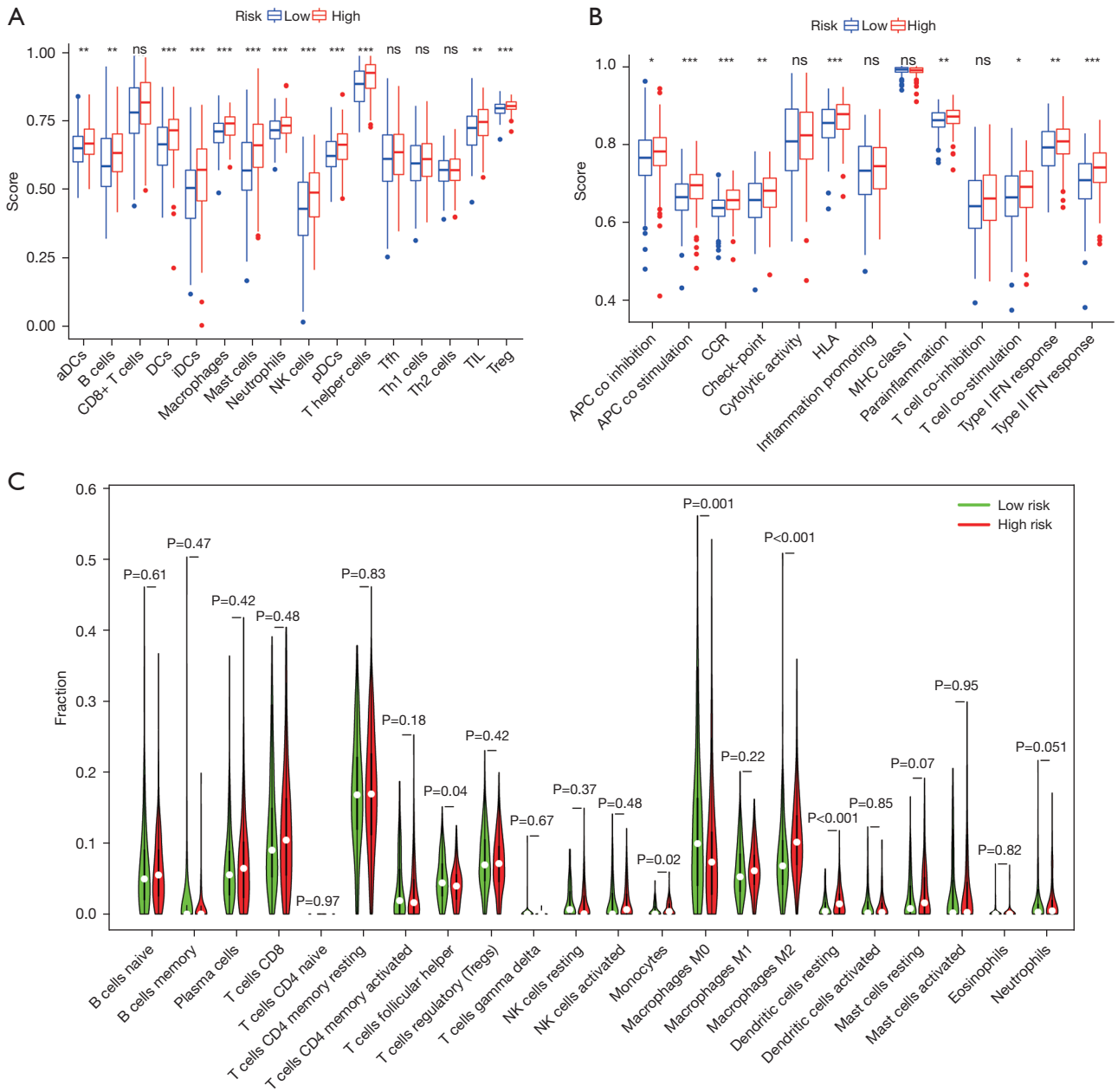

Figure 11 Immune cell infiltration and immune-related functions in different risk groups. The levels of immune cell infiltration in different risk groups were analyzed using the ssGSEA algorithm, and the results are presented in (A). The association between risk scores and 13 immune-related functions was also evaluated as shown in (B). Further, differences in 22 types of immune cells between different risk groups were determined using the Wilcoxon rank-sum test as presented in (C). *, P<0.05; **, P<0.01; ***, P<0.001; ns, non-significant. ssGSEA, single-sample gene set enrichment analysis; aDCs, activated dendritic cells; iDCs, immature dendritic cells; NK, natural killer; pDCs, plasmacytoid dendritic cells; Tfh, T follicular helper; Th1, T helper type 1; Th2, T helper type 2; TIL, tumor-infiltrating lymphocyte; Treg, T regulatory cell; APC, antigen-presenting cell; CCR, C-C chemokine receptor; HLA, human leukocyte antigen; MHC, major histocompatibility complex; IFN, interferon.

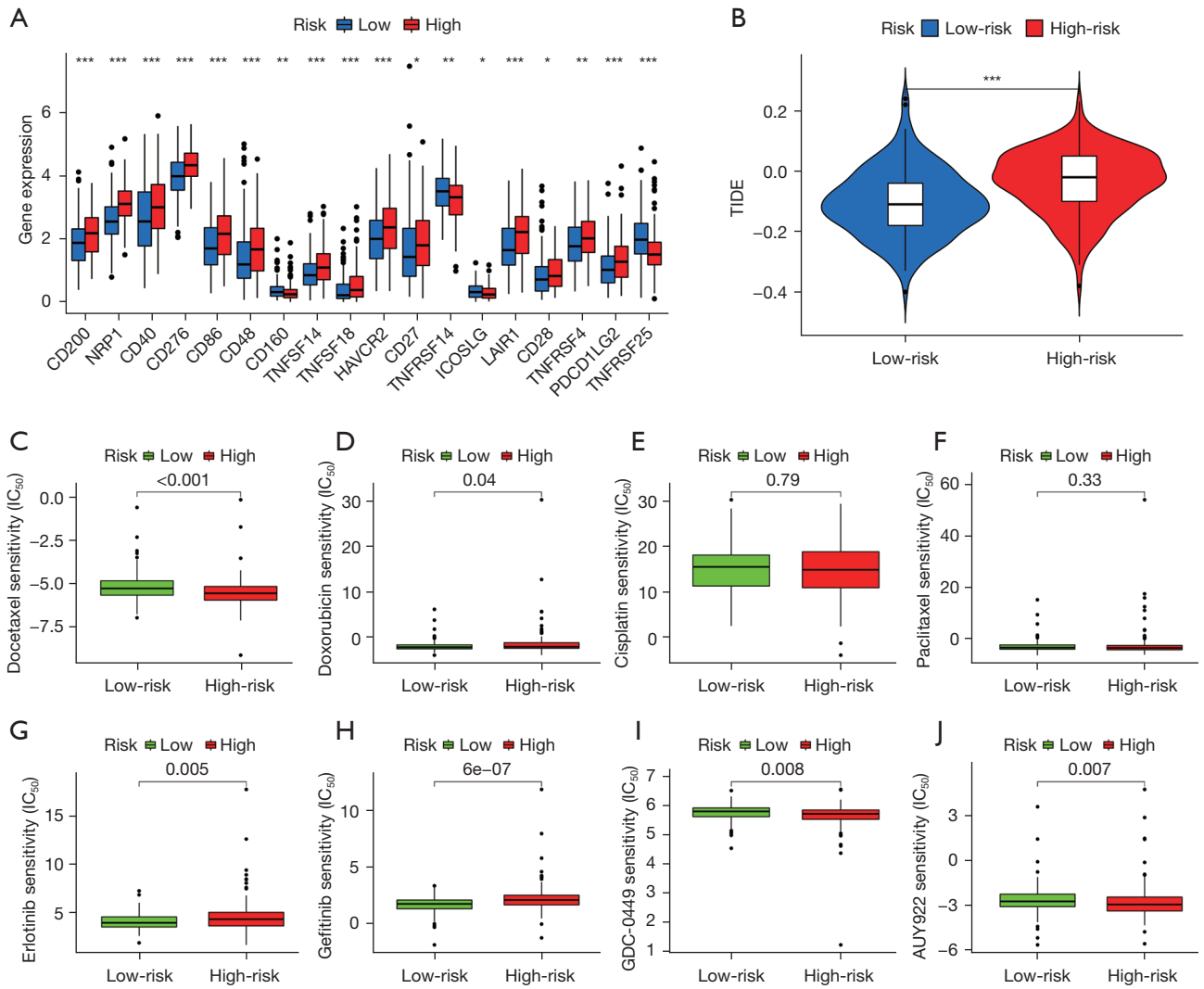

Figure 12 Comparison of immune checkpoints, TIDE module scores, and the sensitivity to chemotherapy and targeted therapy drugs of the high- and low-risk groups. The expression levels of 18 immune checkpoint genes were compared between the high- and low-risk groups, and the results are presented in (A). The red boxes represent high-risk patients; the blue boxes represent low-risk patients. In addition, the efficacy of anti-PD1 or anti-CTLA4 was predicted using the online software "TIDE" for each GC subgroup, and a higher TIDE score indicated a higher likelihood of tumor immune escape and a poorer response to immunotherapy as shown in (B). The IC_{50} values for (C) docetaxel, (D) doxorubicin, (E) cisplatin, (F) paclitaxel, (G) erlotinib, (H) gefitinib, (I) GDC-0449, and (J) AUY922 in the high- and low-risk groups. *, P<0.05; **, P<0.01; ***, P<0.001. GC, gastric cancer; TIDE, tumor immune dysfunction and exclusion; IC_{50}, half-maximal inhibitory concentration.

levels of AC005586.1 and AP001528.2 did not differ significantly between the tumor and non-tumor tissues; however, this might be related to the small sample size of the study. Taking these findings together, we validated the *in silico* results using GC cell lines and an independent GC cohort.

Discussion

It is expected that the eradication of *Helicobacter pylori* will largely prevent GC (27). However, there are still more than 1 million new cases of GC worldwide each year, making it a significant public health burden (28). For advanced GC, the

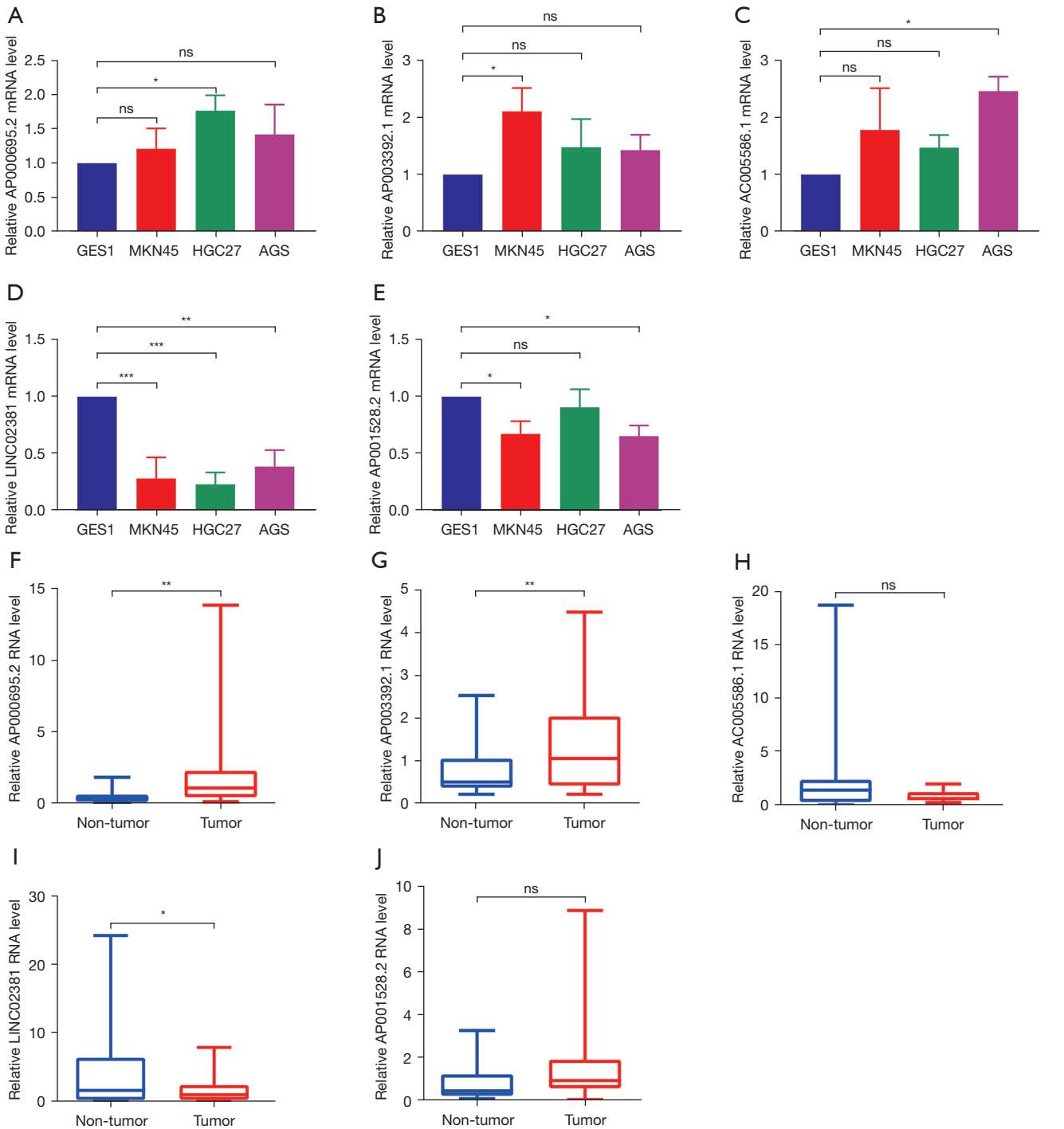

Figure 13 The qRT-PCR assays of the expression levels of the five lncRNAs in GC cell lines and an independent validation cohort of 30 GC samples. The mRNA levels of (A) AP000695.2, (B) AP003392.1, (C) AC005586.1, (D) LINC02381, and (E) AP001528.2 were compared between the GC cell lines (MKN45, HGC27, and AGS) and human normal gastric mucosal cells (GES1). A one-way analysis of variance was used to test the differences between the groups, and an adjusted P value for multiple comparisons <0.05 indicated statistical significance. The RNA levels of (F) AP000695.2, (G) AP003392.1, (H) AC005586.1, (I) LINC02381, and (J) AP001528.2 were compared between the tumor and non-tumor tissues. An unpaired *t*-test was used to test the differences between groups. *, P<0.05; **, P<0.01; ***, P<0.001; ns, non-significant. GC, gastric cancer; lncRNA, long non-coding RNA; mRNA, messenger RNA; qRT-PCR, quantitative reverse-transcription polymerase chain reaction.

5-year survival rate after surgical treatment is only about 18–50% (24). Therefore, there is still a need to find new markers for the prevention and treatment of GC (29).

Senescent cells have recently been found to alter patient prognosis (6); when tumor tissues contain more senescent cells, patients tend to have lower OS rates and shorter recurrence-free survival (30). Conversely, research has shown that the elimination of senescent cells expressing the cell cycle inhibitor $p16^{INK4a+}$ significantly reduced the occurrence of spontaneous carcinogenesis in mice (31). Some biomarkers, such as beta-galactosidase activity, are currently employed to characterize senescent cells; however, these classifications are debatable (12,32,33). LncRNAs are currently prospective indicators for GC cell senescence; however, the current research on lncRNAs is limited (13,34). Thus, we extensively investigated senescent lncRNAs in the context of GC to characterize senescent cells in the GC TME. Both AP000695.2 (35-37) and AP003392.1 (38), which were included in our SenLncSig model, were previously identified as prognostic biomarkers of GC. LINC02381 (39) inhibits GC progression by regulating the Wnt signaling pathway. The qRT-PCR assays of our GC cell lines and GC samples confirmed that AP000695.2 and AP003392.1 were upregulated, while LINC02381 was downregulated in the tumor cells and tissues, which supports previous research on GC cell lines and tissues (37-39).

Currently, most animal models are established in 4–8-week-old mice rather than more appropriate cancer modelling animals, such as aged mice (26). This observation may partly elucidate why numerous promising preclinical treatments fail in the clinical trial stages. Further, the AUC accuracy of our SenLncSig model (*Figure 4B*) is equivalent to that of other studies (15,36-38,40) that used TCGA data to construct lncRNA prediction models. These findings demonstrate that senescent cells present in the TME contribute to the prognosis of GC and hold a similar value as other biomarkers.

Research into the use of immunotherapy to treat GC is currently in full swing. The KEYNOTE-059 trial investigated the efficacy of pembrolizumab (an anti-PD-1 antibody) monotherapy in previously treated patients with advanced GC, and found that it achieved an 11.6% objective response rate (41). Additionally, in a similar GC cohort, the ATTRACTION-2 trial evaluated the efficacy of another anti-PD-1 antibody, nivolumab, and achieved an objective response rate of 11% (42). These findings support the notion that adequate patient selection has a significant impact on the effectiveness of immunotherapy.

Fortunately, senescence has become an important parameter that has recently been considered for screening patients who may benefit from ICI therapy in both preclinical and clinical retrospective studies. In a mouse model of melanoma, anti-PD-1, anti-PD-L1, and anti-CTLA4 were effective in treating young mice, but anti-PD-L1 was not effective in treating aged mice (43). Conversely, the efficacy of anti-PD-1 treatment was found to be more effective in senior patients than young patients (44). Similarly, the current study discovered a link between cellular senescence and the TME.

As *Figures 11,12A,12B* show, the SenLncSig high-risk group had significantly higher levels of anti-tumor immune cell infiltration, immune pathway activation, and expression of the majority of immune checkpoints than the low-risk group. These findings suggest that patients with high-risk scores may be more responsive to immunotherapy. Notably, research has found that pre-existing or recoverable anti-tumor immune responses in the TME contribute to the success of immunological treatment (22). This theory may explain why high-risk groups, as well as high-immune-infiltration groups, are more likely to benefit from immunological treatment. Conversely, a high TMB implies the production of tumor neoantigens that may potentially activate $CD8^+$ T cells and thus destroy tumor cells (45). This could explain why a better prognosis was found in the low-risk group, in which the individuals had both a higher TMB rating (*Figure 10C*) and a higher overall rate of driver gene mutations (*Figure 10B*). These findings highlight the characteristics of cellular senescence and its effects on the tumor immune microenvironment, and could inform potential future tumor immunotherapy strategies that focus on cellular senescence treatment.

Senescent stromal cell populations are another factor affecting cancer phenotypes. Most cancer treatment strategies have relied on inducing cellular senescence and thus programmed cell death. However, despite treatment-induced senescence, stromal cells in the TME continue to release SASPs to maintain tumor survival (6,46). For example, the presence of chemotherapy or radiation-induced senescent endothelial cells greatly increases the survival and progression of breast cancer cells through the secretion of CXCL11 and VCAM1 (47,48). Because the SenLncSig model fully accounts for cellular senescence markers in the TME, it may be feasible to choose individuals who benefit from chemotherapy regimens based on the senescent condition of the TME, which may have implications for future customized medication selection.

The current study had two major limitations. First, only the TCGA data set, which comprised both the discovery and validation sets, was used in our study, and no external data sets were used. As far as we know, unlike breast cancer [for which there are the Molecular Taxonomy of Breast Cancer International Consortium (METABRIC) and International Cancer Genome Consortium (ICGC) data sets] and glioma [for which there are the Chinese Glioma Genome Atlas (CGGA) data sets], with the exception of the TCGA data set, few other public data sets with such a large sample size and complete prognostic data are available for GC. There are several GC data sets in the Gene Expression Omnibus database; however, these data sets use a coding gene array platform rather than a next-generation sequencing or lncRNA array platform. As a result, we were unable to validate TCGA-generated lncRNA model on even one external GC data set. Second, molecular mechanism studies are required to identify the effects of the SenLncSig lncRNAs.

Conclusions

In summary, this study established a SenLncSig lncRNA model that can be used to predict the prognosis of GC. It also constructed a nomogram with the SenLncSig model for the GC prognostic analysis. Notably, the SenLncSig model could potentially predict the efficacy of immunotherapy.

Acknowledgments

The authors would like to thank BioMed Proofreading® LLC Co., Ltd for their language editing support.
Funding: This project received funding from the Science and Technology Program of Guangzhou (No. 2024A03J0493 to J.S.).

Footnote

Reporting Checklist: The authors have completed the TRIPOD reporting checklist. Available at https://jgo.amegroups.com/article/view/10.21037/jgo-24-792/rc

Data Sharing Statement: Available at https://jgo.amegroups.com/article/view/10.21037/jgo-24-792/dss

Peer Review File: Available at https://jgo.amegroups.com/article/view/10.21037/jgo-24-792/prf

Conflicts of Interest: All authors have completed the ICMJE uniform disclosure form (available at https://jgo.amegroups.com/article/view/10.21037/jgo-24-792/coif). J.S. reports funding from the Science and Technology Program of Guangzhou (No. 2024A03J0493). The other authors have no conflicts of interest to declare.

Ethical Statement: The authors are accountable for all aspects of the work in ensuring that questions related to the accuracy or integrity of any part of the work are appropriately investigated and resolved. The study was conducted in accordance with the Declaration of Helsinki (as revised in 2013). This study was authorized by the Research Ethics Committee of the Sixth Affiliated Hospital of Sun Yat-sen University (protocol code: 2020ZSLYEC-284). Written informed consent was obtained from all the participants.

References

1. Siegel RL, Giaquinto AN, Jemal A. Cancer statistics, 2024. CA Cancer J Clin 2024;74:12-49.
2. Wang Z, Han W, Xue F, et al. Nationwide gastric cancer prevention in China, 2021-2035: a decision analysis on effect, affordability and cost-effectiveness optimisation. Gut 2022;71:2391-400.
3. Guan WL, He Y, Xu RH. Gastric cancer treatment: recent progress and future perspectives. J Hematol Oncol 2023;16:57.
4. Joshi SS, Badgwell BD. Current treatment and recent progress in gastric cancer. CA Cancer J Clin 2021;71:264-79.
5. Nakamura Y, Kawazoe A, Lordick F, et al. Biomarker-targeted therapies for advanced-stage gastric and gastro-oesophageal junction cancers: an emerging paradigm. Nat Rev Clin Oncol 2021;18:473-87.
6. Hanahan D. Hallmarks of Cancer: New Dimensions.

Cancer Discov 2022;12:31-46.
7. Kowald A, Passos JF, Kirkwood TBL. On the evolution of cellular senescence. Aging Cell 2020;19:e13270.
8. Wang B, Kohli J, Demaria M. Senescent Cells in Cancer Therapy: Friends or Foes? Trends Cancer 2020;6:838-57.
9. Birch J, Gil J. Senescence and the SASP: many therapeutic avenues. Genes Dev 2020;34:1565-76.
10. Lian J, Yue Y, Yu W, et al. Immunosenescence: a key player in cancer development. J Hematol Oncol 2020;13:151.
11. Wei L, Sun J, Zhang N, et al. Noncoding RNAs in gastric cancer: implications for drug resistance. Mol Cancer 2020;19:62.
12. Casella G, Munk R, Kim KM, et al. Transcriptome signature of cellular senescence. Nucleic Acids Res 2019;47:7294-305.
13. Li Y, Li D, Zhao M, et al. Long noncoding RNA SNHG6 regulates p21 expression via activation of the JNK pathway and regulation of EZH2 in gastric cancer cells. Life Sci 2018;208:295-304.
14. Chen S, Li X, Zhang J, et al. Six mutator-derived lncRNA signature of genome instability for predicting the clinical outcome of colon cancer. J Gastrointest Oncol 2021;12:2157-71.
15. Chen S, Ben X, Guo L, et al. Identification of lncRNAs based on different patterns of immune infiltration in gastric cancer. J Gastrointest Oncol 2022;13:102-16.
16. Zeng X, Shapaer T, Tian J, et al. Identifying a CD8T cell signature in the tumor microenvironment to forecast gastric cancer outcomes from sequencing data. J Gastrointest Oncol 2024;15:2067-78.
17. Chen R, Jiang L. A novel m6A/m5C/m1A/m7G-related classification and risk signature predicts prognosis and reveals immunotherapy inclination in gastric cancer. Transl Cancer Res 2024;13:3285-98.
18. Liu Z, Yang M, Shu H, et al. A novel prognostic and therapeutic target biomarker based on complement-related gene signature in gastric cancer. Transl Cancer Res 2023;12:3565-80.
19. Song W, Zhu J, Li C, et al. Identification and validation of an epithelial-mesenchymal transition-related lncRNA pairs prognostic model for gastric cancer. Transl Cancer Res 2023;12:1196-209.
20. Avelar RA, Ortega JG, Tacutu R, et al. A multidimensional systems biology analysis of cellular senescence in aging and disease. Genome Biol 2020;21:91.
21. Mayakonda A, Lin DC, Assenov Y, et al. Maftools: efficient and comprehensive analysis of somatic variants in cancer. Genome Res 2018;28:1747-56.
22. Rooney MS, Shukla SA, Wu CJ, et al. Molecular and genetic properties of tumors associated with local immune cytolytic activity. Cell 2015;160:48-61.
23. Newman AM, Liu CL, Green MR, et al. Robust enumeration of cell subsets from tissue expression profiles. Nat Methods 2015;12:453-7.
24. In H, Ravetch E, Langdon-Embry M, et al. The newly proposed clinical and post-neoadjuvant treatment staging classifications for gastric adenocarcinoma for the American Joint Committee on Cancer (AJCC) staging. Gastric Cancer 2018;21:1-9.
25. Huang E, Fu J, Yu Q, et al. CircRNA hsa_circ_0004771 promotes esophageal squamous cell cancer progression via miR-339-5p/CDC25A axis. Epigenomics 2020;12:587-603.
26. Mlecnik B, Bindea G, Angell HK, et al. Integrative Analyses of Colorectal Cancer Show Immunoscore Is a Stronger Predictor of Patient Survival Than Microsatellite Instability. Immunity 2016;44:698-711.
27. Zhou WT, Jin WL. B7-H3/CD276: An Emerging Cancer Immunotherapy. Front Immunol 2021;12:701006.
28. Ralser DJ, Klümper N, Gevensleben H, et al. Molecular and Immune Correlates of PDCD1 (PD-1), PD-L1 (CD274), and PD-L2 (PDCD1LG2) DNA Methylation in Triple Negative Breast Cancer. J Immunother 2021;44:319-24.
29. Jiang P, Gu S, Pan D, et al. Signatures of T cell dysfunction and exclusion predict cancer immunotherapy response. Nat Med 2018;24:1550-8.
30. Fane M, Weeraratna AT. How the ageing microenvironment influences tumour progression. Nat Rev Cancer 2020;20:89-106.
31. Sexton RE, Al Hallak MN, Diab M, et al. Gastric cancer: a comprehensive review of current and future treatment strategies. Cancer Metastasis Rev 2020;39:1179-203.
32. Thrift AP, El-Serag HB. Burden of Gastric Cancer. Clin Gastroenterol Hepatol 2020;18:534-42.
33. Guo Y, Qu Z, Li D, et al. Identification of a prognostic ferroptosis-related lncRNA signature in the tumor microenvironment of lung adenocarcinoma. Cell Death Discov 2021;7:190.
34. Sanfeliu-Redondo D, Gibert-Ramos A, Gracia-Sancho J. Cell senescence in liver diseases: pathological mechanism and theranostic opportunity. Nat Rev Gastroenterol Hepatol 2024;21:477-92.
35. Maggiorani D, Le O, Lisi V, et al. Senescence drives immunotherapy resistance by inducing an immunosuppressive tumor microenvironment. Nat Commun 2024;15:2435.

36. Camacho-Encina M, Booth LK, Redgrave RE, et al. Cellular Senescence, Mitochondrial Dysfunction, and Their Link to Cardiovascular Disease. Cells 2024;13:353.
37. Reimann M, Lee S, Schmitt CA. Cellular senescence: Neither irreversible nor reversible. J Exp Med 2024;221:e20232136.
38. Paronetto MP, Dimauro I, Grazioli E, et al. Exercise-mediated downregulation of MALAT1 expression and implications in primary and secondary cancer prevention. Free Radic Biol Med 2020;160:28-39.
39. Zhang S, Zheng N, Chen X, et al. Establishment and Validation of a Ferroptosis-Related Long Non-Coding RNA Signature for Predicting the Prognosis of Stomach Adenocarcinoma. Front Genet 2022;13:818306.
40. Chen D, Wang M, Xu Y, et al. A Novel Autophagy-Related lncRNA Prognostic Signature Associated with Immune Microenvironment and Survival Outcomes of Gastric Cancer Patients. Int J Gen Med 2021;14:6935-50.
41. Zha Z, Zhang P, Li D, et al. Identification and Construction of a Long Noncoding RNA Prognostic Risk Model for Stomach Adenocarcinoma Patients. Dis Markers 2021;2021:8895723.
42. Wei J, Zeng Y, Gao X, et al. A novel ferroptosis-related lncRNA signature for prognosis prediction in gastric cancer. BMC Cancer 2021;21:1221.
43. Jafarzadeh M, Soltani BM. Long Noncoding RNA LOC400043 (LINC02381) Inhibits Gastric Cancer Progression Through Regulating Wnt Signaling Pathway. Front Oncol 2020;10:562253.
44. Wang Y, Zhang H, Wang J. Discovery of a novel three-long non-coding RNA signature for predicting the prognosis of patients with gastric cancer. J Gastrointest Oncol 2020;11:760-9.
45. Fuchs CS, Doi T, Jang RW, et al. Safety and Efficacy of Pembrolizumab Monotherapy in Patients With Previously Treated Advanced Gastric and Gastroesophageal Junction Cancer: Phase 2 Clinical KEYNOTE-059 Trial. JAMA Oncol 2018;4:e180013.
46. Kang YK, Boku N, Satoh T, et al. Nivolumab in patients with advanced gastric or gastro-oesophageal junction cancer refractory to, or intolerant of, at least two previous chemotherapy regimens (ONO-4538-12, ATTRACTION-2): a randomised, double-blind, placebo-controlled, phase 3 trial. Lancet 2017;390:2461-71.
47. Padrón Á, Hurez V, Gupta HB, et al. Age effects of distinct immune checkpoint blockade treatments in a mouse melanoma model. Exp Gerontol 2018;105:146-54.
48. Kugel CH 3rd, Douglass SM, Webster MR, et al. Age Correlates with Response to Anti-PD1, Reflecting Age-Related Differences in Intratumoral Effector and Regulatory T-Cell Populations. Clin Cancer Res 2018;24:5347-56.

(English Language Editor: L. Huleatt)

Cite this article as: Shi J, Hou Z, Fan L, Hu C, Ma N, Huang E. Development and experimental validation of a senescence-related long non-coding RNA signature for prognostic prediction and immune microenvironment characterization in gastric cancer patients. J Gastrointest Oncol 2024;15(6):2413-2436. doi: 10.21037/jgo-24-792